Model-based estimation of Liquid Flows in the Blast Furnace Hearth and Taphole

Lei Shao

Doctor of Technology Thesis

Thermal and Flow Engineering Laboratory
Department of Chemical Engineering
Åbo Akademi University

Turku/Åbo, Finland, 2013

MODEL-BASED ESTIMATION OF LIQUID FLOWS IN THE BLAST FURNACE HEARTH AND TAPHOLE

Lei Shao

Doctor of Technology Thesis

Thermal and Flow Engineering Laboratory
Department of Chemical Engineering
Åbo Akademi University

Turku/Åbo, Finland, 2013

ISBN 978-952-12-2941-1
Painosalama Oy – Turku, Finland 2013

Preface

The work reported in this thesis was conducted at the Thermal and Flow Engineering Laboratory of Åbo Akademi University in Finland during the years 2009-2013. The research was mainly supported by the State Scholarship Fund of China, a grant from the European Coal and Steel Community within the project "Improvement of Hearth Drainage Efficiency and Refractory Life for High BF Productivity and a Well Adjusted Reductant Injection Rate at Varying Coke Quality", the Åbo Akademi Foundation and Svenska Tekniska Vetenskapsakademien i Finland. I gratefully acknowledge the financial support which has enabled me to put full-time efforts into the thesis work.

I would like to express my sincere gratitude to my supervisor Prof. Henrik Saxén for constantly believing in me and encouraging me. I truly appreciate the freedom he has given me in my research. Also, there are a number of other people I wish to thank for their help during my time working on this thesis. In particular, I would like to acknowledge Affi and Vivéca for their help of office-related arrangement and payment processing. A special thank you goes to Calle, who has been helping me in many ways making my life easy in Finland. In addition, a lot of people have supported me in some less tangible ways, but still significantly. I would like to thank Prof. Masakata Shimizu, Prof. Kazuya Kunitomo, Mr. Takayuki Maeda and Mr. Ko-ichiro Ohno for their kind hospitality when I visited Kyushu University of Japan as a guest researcher in late 2012.

I would like to thank my wife Shan for all the love and support she has given me. I also owe a big thank you to Prof. Seppo Louhenkilpi in Aalto University for allowing Shan to work remotely in Turku, bringing me the really invaluable things in my life. Finally, I wish to thank my parents and parents-in-law for their everlasting love.

Turku/ Åbo, September, 2013
Lei Shao

Abstract

This thesis presents a set of methods and models for estimation of iron and slag flows in the blast furnace hearth and taphole. The main focus was put on predicting taphole flow patterns and estimating the effects of various taphole conditions on the drainage behavior of the blast furnace hearth. All models were based on a general understanding of the typical tap cycle of an industrial blast furnace. Some of the models were evaluated on short-term process data from the reference furnace. A computational fluid dynamics (CFD) model was built and applied to simulate the complicated hearth flows and thus to predict the regions of the hearth exerted to erosion under various operating conditions. Key boundary variables of the CFD model were provided by a simplified drainage model based on the first principles. By examining the evolutions of liquid outflow rates measured from the furnace studied, the drainage model was improved to include the effects of taphole diameter and length. The estimated slag delays showed good agreement with the observed ones. The liquid flows in the taphole were further studied using two different models and the results of both models indicated that it is more likely that separated flow of iron and slag occurs in the taphole when the liquid outflow rates are comparable during tapping. The drainage process was simulated with an integrated model based on an overall balance analysis: The high in-furnace overpressure can compensate for the resistances induced by the liquid flows in the hearth and through the taphole. Finally, a recently developed multiphase CFD model including interfacial forces between immiscible liquids was developed and both the actual iron-slag system and a water-oil system in laboratory scale were simulated. The model was demonstrated to be a useful tool for simulating hearth flows for gaining understanding of the complex phenomena in the drainage of the blast furnace.

Refereat

I avhandlingen har en uppsättning metoder och matematiska modeller utvecklats för estimering av järn- och slaggströmmar i masugnens ställ och tapphål. Arbetets huvudsakliga tonvikt var förlagd till att prediktera strömningsförloppet i tapphålet och att uppskatta effekten av tapphålsförhållanden på masugnsställets dränering. Modellerna grundar sig på en allmänt accepterad uppfattning av förloppen vid tappning av industriella masugnar. Några av modellerna utvärderades och verifierades på basis av korttidsdata från en masugn som användes som referens för arbetet. En numerisk strömningsmodell (CFD, computational fluid dynamics) utvecklades och tillämpades för att simulera de komplexa flödesmönstren. Resultaten visade att modellen kunde detektera de delar av masugnsstället som är mest utsatta för slitage under tappningarna. Viktiga randvillkor för CFD-modellen genererades med en förenklad simuleringsmodell av tappcykeln baserad på mass- och energibalanser. Modellen vidareutvecklades därefter för att beakta längden och diametern hos tapphålet. De slaggfördröjningar modellen förutspådde befanns överensstämma väl med fördröjningar som observerats i praktiken. Smältornas flöden i tapphålet studerades noggrannare med hjälp av två olika numeriska modeller som utvecklades för ändamålet. Resultaten visade att smältorna flödar företrädelsevis skiktade i tapphålet under en betydande del av tappningen. Tappningsförloppet simulerades härvid med en integrerad modell baserad på totalbalanser, där det höga övertrycket i masugnsstället uppväger det tryckfall som förorsakas av smältornas strömning genom koksbädden och genom tapphålet. Slutligen tillämpades en nyligen utvecklad numerisk modell för flerfasströmning, som beaktar krafter vid gränsskiktet mellan de oblandbara faserna, för att beskriva strömningsmönstren i tapphålet. Modellen tillämpades på det föreliggande systemet med järn och slagg, men även på fall med vatten och olja för vilka experimentella resultat rapporterats i litteraturen. Modellen visade sig vara användbar för simulering av de komplexa strömningsförloppen under masugnens tappning.

Contribution of the author and list of publications

In addition to the present summary, the following papers are included in the thesis as appendices:

I. Lei Shao and Henrik Saxén (2012)
"Numerical Prediction of Iron Flow and Bottom Erosion in the Blast Furnace Hearth"
Steel Research International, Vol. 83, pp. 878-885.

II. Lei Shao and Henrik Saxén (2012)
"Model of Blast Furnace Hearth Drainage"
Steel Research International, Vol. 83, pp. 197-204.

III. Lei Shao and Henrik Saxén (2013)
"A Simulation Study of Two-liquid Flow in the Taphole of the Blast Furnace"
ISIJ International, Vol. 53, pp. 988-994.

IV. Lei Shao and Henrik Saxén (2013)
"Flow Patterns of Iron and Slag in the Blast Furnace Taphole"
ISIJ International, Vol. 53, pp. 1756-1762.

V. Lei Shao and Henrik Saxén (2011)
"A Simulation Study of Blast Furnace Hearth Drainage using a Two-phase Flow Model of the Taphole"
ISIJ International, Vol. 51, pp. 228-235.

VI. Lei Shao and Henrik Saxén (2013)
"Simulation Study of Blast Furnace Drainage using a Two-fluid Model"
Industrial & Engineering Chemistry Research, Vol. 52, pp. 5479-5488.

The author of this thesis is the main contributor of the six papers above. He has written the draft of each paper and has later revised the manuscript with his supervisor. All the CFD simulations described in the papers were performed by the author. He also established a majority of other mathematical models shown in the papers.

Table of Contents

Chapter 1
Introduction

There has been speculation about the demise of blast furnaces along with the development of many alternative (direct reduction and coke-free smelting) processes. These new technologies can be summarized by noting that several have been abandoned, some are still under development but not fully proven while the others are only being adopted in appropriate niches. The world's production of pig iron and crude steel during the years 2000-2012, shown in Table 1, clearly shows that almost 70 % (or more) of the total crude steel in the world was produced from blast furnace pig iron since the start of the 21st century. It is thus safe to say that blast furnace is still the primary producer of raw material for large-scale steelmaking industry. In order to keep its position and to response to the challenges from the alternative technologies, the blast furnace should be amenable to continuous development and improvement to achieve the goals of higher productivity, lower coke consumption, less environmental impact and longer campaign life.

The state of the hearth has by many researchers been identified to play the most important role for stable furnace operation and long campaign life. This lowest region is exposed to molten iron and slag which are in direct contact with the refractory materials, causing severe erosion and chemical and thermal attack of the hearth lining. The most aggressive environment in a furnace hearth is usually found in the vicinity of the taphole(s), which is subject to high thermal stresses and liquid flow velocities. The taphole management (integrated with other operational guidance techniques) was reportedly crucial in hearth performance and, hence, in the overall furnace operation (Nightingale et al., 2001; Tanzil et al., 2001, 2004). However, the prevailing conditions in the taphole have not been well examined and strong simplifications and assumptions have been applied in the few studies of the region, which is one of the motivations behind the work presented in this thesis.

Table 1. World's production of (blast furnace) pig iron and crude steel during the years 2000-2012†

Year	Pig Iron [Mt]	Crude Steel [Mt]	Ratio produced in BF [%]
2000	576.25	848.94	67.88
2001	586.95	851.07	68.97
2002	611.13	904.05	67.60
2003	669.99	969.92	69.08
2004	719.20	1061.25	67.77
2005	800.82	1146.58	69.84
2006	881.12	1248.99	70.55
2007	961.58	1347.00	71.39
2008	951.17	1341.21	70.92
2009	934.66	1235.84	75.63
2010	1035.41	1428.71	72.47
2011	1082.07	1490.06	72.62
2012	1100.00	1510.22	72.84

† The statistics have been published on *www.worldsteel.org*.

The summary of this thesis includes a brief description of the blast furnace process and the main phenomena in the hearth and taphole. Various investigations and modeling methods in the related field are also reviewed. Finally, the models developed in the present thesis are illustrated by a few examples.

Chapter 2
Blast Furnace Background

In this chapter the ironmaking process of the blast furnace is briefly introduced and the focus is put on describing the hearth region and some associated phenomena which are studied in the thesis.

2.1 Overview of blast furnace process

The blast furnace is essentially a huge countercurrent heat exchanger and chemical reactor in which pig iron is produced from iron-bearing ore. The internal state of blast furnaces has been revealed since 1970s when extensive dissection investigations were carried out on various quenched furnaces in Japan (Omori, 1987). A schematic view of blast furnace is shown in Fig. 1, where some of the terminology used throughout this thesis is also depicted.

The raw materials consisting of iron ore (pellets and/or sinter), coke and flux (limestone and quartzite) are supplied at the top by utilizing a charging system with bell or bell-less design. A layer-structured burden is formed in the furnace as the ore (together with the flux) and coke are charged in separate dumps. Coke is the main fuel used and has several metallurgical functions in blast furnaces: It supports the burden and provides permeable routes to the liquids and gases in the furnace when other solid phases are softened and melted; it is also a reducing agent and heat source that offers energy for melting solid phases and for endothermic reactions in the furnace.

In the lower section of the furnace, oxygen enriched hot air and additional fuels, such as oil, pulverized coal and natural gas, are blown in through a number of *tuyeres* equipped around the furnace peripheral (cf. Fig. 1). The *raceway* is formed in front of each tuyere

where coke and other fuels combust to produce large amount of heat and reducing gas. The hot gas (~ 2000 °C) travels upwards through the *bosh* and *shaft*, gradually heating and reducing the descending burden. As a result, the burden stays in a "lumpy" stage before being softened and eventually melted, forming the *cohesive zone*. In general, the shape of the cohesive zone is determined by the raceway conditions and burden distribution (ore/coke ratio and material size) in the furnace. It has great influence on the furnace operation, including fuel rate, burden movement and gas distribution as the ore layers in the cohesive zone become virtually impermeable and the ascending gas is forced to pass through the coke slits (cf. Fig. 1).

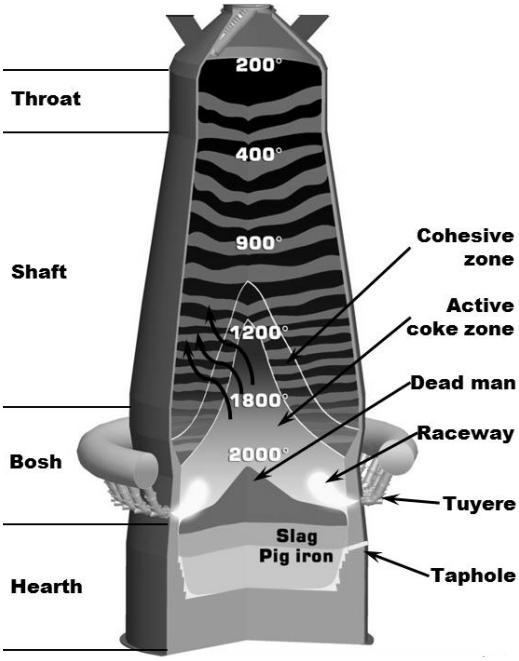

Figure 1. Schematic view of the internal structure of a blast furnace.

From the cohesive zone downwards, the only solid present is coke. Liquid iron and slag dripping from the lower surface of the cohesive zone trickle down through the *active coke zone* and a central, near stagnant coke bed, the *dead man*. The molten liquids finally accumulate in the *hearth*, where they are stored and drained out through the *taphole(s)*.

2.2 Hearth and dead man

The hearth is the lowest, but the most important part of a blast furnace. The campaign life of a furnace considerably depends on its hearth durability: Other parts of blast furnaces can be relined or replaced in a relatively short period. However, relining a broken hearth takes much longer time and it often escalates to a complete revamp (Raipala, 2003). The hearth sidewall and bottom are usually constructed of carbon-based blocks or bricks combined with high quality ceramics. The hearth linings are equipped with a number of thermocouples and cooling elements.

As shown in Fig. 1, the dead man is situated beneath the active coke zone and (mostly) below the raceways. The upper part of the dead man is cone-shaped with a rounded top in the region between the raceways (Nishio et al., 1977). The inclination from the dead-man apex to the raceways is approximately the same as the repose angle of the charged coke (Raipala, 2003). The hearth is mainly occupied by a coke bed, which is a part of the dead man extending from the tuyere level. Henceforth, the hearth coke bed and dead man will be used as synonyms even though the dead man is a slightly broader concept.

Molten iron and slag dripping from the cohesive zone accumulate in the empty spaces of the dead man. As a result of gravity, the liquids segregate into two different layers with the heavier iron on the bottom and the lighter slag on the top. As both iron and slag continuously drip down from the cohesive zone, the iron droplets must sink through the slag layer to the bottom. The top layer therefore consists of a mix of slag and iron droplets (Desai, 1993). The porosity of the dead man is between 0.3 and 0.5 (Kanbara et al., 1977), which indicates that only 30-50 % of the total volume is available for the liquids if the dead man fully fills the hearth. In fact, the dead man may either sit on the bottom of the hearth, or floats partly or completely in the liquid bath if the buoyancy force of the liquids is sufficient to lift the dead man. A partly floating dead man sits on the central hearth bottom and gives rise to an annular coke-free zone at the hearth edges, which offers little flow resistance when the hearth is drained. Therefore, a circumferential

flow is formed, being the main reason for the “elephant-foot”-shaped wear in the hearth (Shibata et al., 1990; Preuer and Winter, 1993).

2.3 Drainage of iron and slag

The drainage, also referred to as casting or tapping, is a process that removes liquid iron and slag from the blast furnace hearth. The drainage process critically determines the in-furnace gas pressure and residual amounts of iron and slag in the hearth. Poor hearth drainage usually leads to unstable furnace operation which is generally connected to marked losses in furnace productivity and campaign life. An inefficient drainage also gives rise to excessive accumulation of liquids and thus high liquid levels in the hearth. If the liquid (slag) approaches the tuyeres level, the reducing gas flow in the bosh is severely disturbed, often resulting in irregular burden descent known as hanging and slipping (Fukutake and Okabe, 1974).

A tap cycle begins as the taphole is drilled open and it is terminated by plugging the taphole with clay when the furnace gas bursts out. At the end of the tap, the *gas-slag interface* tilts down towards the taphole and a considerable amount of slag remains above the taphole level. The iron phase can be drained from levels below the taphole because of the large pressure gradient that develops near the taphole in the viscous slag phase. The average *slag-iron interface* is therefore lower than the taphole level (Tanzil et al., 1984). Depending on a number of factors, such as liquid production rates, hearth (effective) volume and tapping strategies, the initial stage of a tap cycle varies and can be categorized as follows.

Iron-first: This occurs if the slag-iron interface is above the taphole level when the taphole is drilled open. The tap cycle starts with an outflow of iron only, and slag starts flowing later when the slag-iron interface has descended to the taphole. After this, iron and slag are drained simultaneously until the end of the tap. The time elapsed from the start of the tap until slag enters the runner is called the *slag delay*.

Simultaneous: This pattern appears if the slag-iron interface lies in, or at a finite depth below the taphole when the tapping commences. The high pressure gradient in the slag phase can promote iron flow, or even drags iron up from below the taphole. As a result, iron and slag are drained together during the whole tap.

Slag-first: Opposite to the iron-first pattern, slag flows out initially and iron after a delay. This is because the slag-iron interface is far below the taphole as the tapping begins, and the phenomena can be observed in larger furnaces with multiple tapholes. The pressure gradient caused by the viscous slag is initially inadequate to lift iron up. The slag-first drainage pattern was, e.g., reported by Tanzil et al., (1984) and by Nishioka et al. (2005a, b) for the Chiba No. 6 blast furnace (cf. Fig. 2).

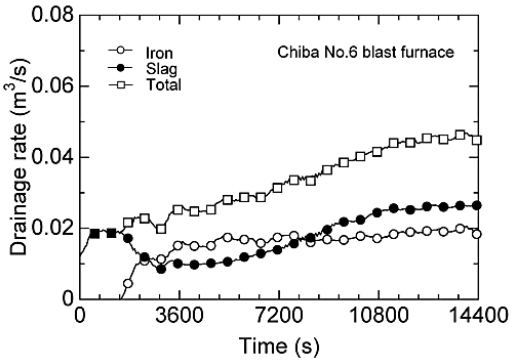

Figure 2. Total, iron and slag drainage rates of Chiba No. 6 blast furnace during a tap (Nishioka et al., 2005a, b).

2.4 Taphole

The taphole is an essential part for the blast furnace. Large furnaces usually have 2-4 tapholes and the drainage is (practically) continuous by periodically drilling and plugging the tapholes; one of the tapholes is always open and two alternate taps usually overlap for some period of time. For medium- or small-size furnace with only one taphole, the time interval between two taps varies from 30 to 90 minutes (Raipala, 2003).

The taphole is exposed to an extremely dynamic environment with high temperature and pressure, frequent drilling and plugging, substantial chemical attack and flow-induced shear. During tapping, the taphole is gradually eroded as the molten liquids flow through it. The greater the wear of the taphole, the greater the change in the liquid flow rates and the greater the variation of liquid levels in the hearth (Nouchi et al., 2005; Nishioka et al., 2005a). To maintain a stable state at the taphole thus facilitating the liquid removal from the hearth, an excess of high quality clay is, in practice, injected in the taphole when a tap is terminated. The taphole clay will accumulate and solidify on the inside of the taphole forming a protective layer with the shape of a "mushroom", which is mainly concentrated directly below the taphole and to a lesser extent sideways and above the taphole. The taphole therefore becomes longer than the depth of the corresponding hearth sidewall through which the taphole is drilled. A longer taphole can drain molten liquids from the inner part of the hearth and the circumferential flow can be suppressed. Also, longer tapholes can result in decreased drainage rates due to the frictional effect and thus lower the taphole clay consumption, which would reduce the overall operational costs (Nightingale, et al., 2001; Tanzil et al., 2001). Recently, the size and shape of the mushroom layer have been reported to have significant effect on the temperature variations of hearth lining during tapping (Swartling et al, 2010, 2012).

Chapter 3
Previous Studies on Drainage Phenomena of Blast Furnace Hearth

The operation of blast furnaces was based almost solely on practical experience and thus the understanding of underlying phenomena was limited until the beginning of 20th century. Today, thanks to extensive research work conducted internationally, the general principles of the blast furnace process have been mostly clarified. In this chapter, some modeling and research methods used to investigate the hearth drainage phenomena are summarized and discussed. The focus is put on models and methods closely related to the work presented in this thesis.

3.1 Investigation and modeling of dead man

The dissection studies of quenched blast furnaces have confirmed the existence of an almost stagnant coke bed in the core of the furnace between raceways and in the hearth (Kanbara et al., 1977; Omori, 1987). The stagnant zone, where coke descends with a strongly reduced velocity, was given the name “dead man” because it was earlier assumed to have no active effect on the functioning of the process (Nishio et al., 1977). However, this assumption has later been proven incorrect as more relevant studies revealed that the dead man plays a key role in the blast furnace operation. A majority of the studies were carried out by using physical and/or mathematical models since the dead man state cannot be directly measured in an operating furnace due to high temperatures, wear, and extremely hostile environment for measuring probes.

3.1.1 Structure and renewal of dead man

The upper part of the dead man is cone-shaped with a rounded top in the region between raceways and it could extend from hearth bottom to far above the tuyeres level. The height of the dead man is dependent upon the furnace size (Nishio et al., 1977) and operating conditions such as coke rate, blast velocity, burden descending and dead-man (coke) renewal rate (Takahashi and Komatsu, 1993; Takahashi et al., 1996). The solid mass/volume losses due to iron-ore (reduction) shrinkage and meltdown strongly affect the solid flow pattern and hence also the dead-man profile. An integrated Computational Fluid Dynamics (CFD) model, which treats each solid phase (iron ore or coke) as a continuum and considers the surface stress caused by the particle-particle kinetic interaction, was developed (Zhang et al., 2002). The model takes into account solid consumptions occurring in the lower part of the blast furnace, such as shrinkage and meltdown of iron ore, gasification, carbonization and combustion of coke. It was found that the dead-man height decreases as the solid consumption rate increases, as shown in Fig. 3. Alternatively, the dead-man profile can be predicted by using the Discrete Element Method (DEM), which calculates the motion of each individual particle in the computational domain on the basis of Newton's law (Kawai and Takahashi, 2004).

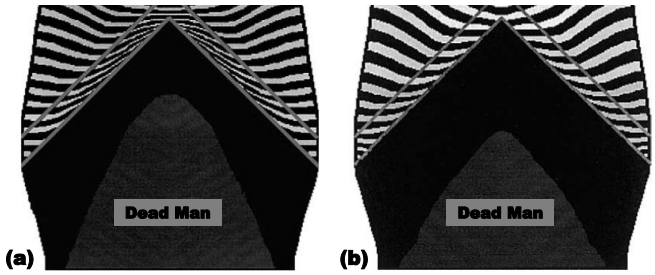

Figure 3. Effect of solid (iron ore and coke) consumption rate on the dead-man profile: The solid consumption rate in (a) is half of that in (b) (Zhang et al., 2002).

The upper boundary of the dead man has been investigated theoretically and experimentally by Takahashi et al. (1993; 1996), who reported that the dead man is surrounded by a quasi-stagnant zone where the charged particles eventually move to the raceway. The dead-man size is sensitive to whether the furnace operation is carried out

with or without Pulverised Coal Injection (PCI). The results showed that the dead man is renewed from a small central inflow region at the top of the dead man. Therefore, good dead-man permeability can be maintained by charging large, high quality coke in the center of the blast furnace. It was also found that the cyclical accumulation and removal of liquids in the hearth due to the tapping operation is closely related to the dead-man renewal process (Kawai and Takahashi, 2004). The dead-man particles move gradually into the raceway as the tapping operation is repeated. The renewal of particles occurs in such a way that the "old" particles are forced to go out of the dead man by the buoyancy force (exerted on the submerged part of the dead man) and the "new" particles come in to fill the dead man through its top surface. Meanwhile, some other dead-man renewal mechanisms, such as carbon solution loss reaction, slag FeO reduction and hot metal carbonization have been studied by different research groups (Sunahara et al., 1993; Kasai et al., 1998; Sun, 2005).

3.1.2 Floating state of dead man

The dead-man state and bottom shape have strong influence on the wear of hearth linings (Vogelpoth et al., 1985) and liquid drainage from blast furnace hearth (Fukutake and Okabe, 1976a, b; Tanzil, 1985; Zulli, 1991). A thorough analysis of the dead-man state can only be made by studying furnaces being revamped or quenched furnaces, which is of course a very expensive method and is only feasible on special occasions. Accurate but local information about the dead-man state in operating furnaces can nowadays be obtained by inserting probes through the tuyeres during scheduled stoppages.

The dead man is submerged in a large liquid bath and is subject to liquid buoyancy exerting on it. As the liquid buoyancy becomes sufficient to lift the dead man, coke-free zones are formed beneath the dead man, hence creating a free passage for liquid flows (Shibata et al., 1990). The dynamic behavior of the dead man as it moves with varying liquid level was investigated by utilizing a three-dimensional scale model (Shinotake et al., 2003). It was found that the movement of the dead man is affected by hysteresis as it ascends and descends in the hearth. The experimental results also showed that the dead man starts floating earlier if air is blown in through the tuyeres. The dead-man bottom

shape is determined by several factors, but in the physical model runs with air blown in through the tuyeres and particles being discharged near the tuyeres, the dead-man bottom was found to assume a profile where it floats higher near the sidewall.

The dead-man state can be estimated by a balance between the force pressing down the dead man and the buoyancy forces of iron and slag in the hearth. The buoyancy force is relatively straightforwardly estimated as it is a function of liquid level and dead-man porosity. However, the downward-acting force, which is usually expressed in the form of a pressure, depends on the furnace conditions, such as burden weight, raceway length, liquid holdup and gas drag (Takahashi et al., 2002; Shinotake et al., 2003). The lower part of a blast furnace is schematically sketched in Fig. 4, where the dead man is divided into two particular regions according to the raceway length, namely, region under raceways and central region.

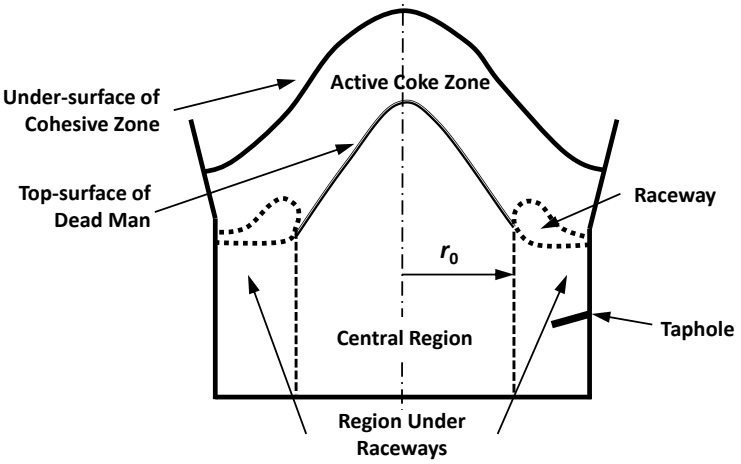

Figure 4. Schematic sketch representing the lower part of a blast furnace.

Tsuchiya et al. (1998) pointed out that the burden weight above the tuyere level is compensated by the lifting pressure of upward flowing gas and the downward-acting pressure under the raceways (i.e., region under raceways) is thus only attributed to the dead-man weight. On the other hand, the downward-acting pressure on the central region was formulated as a function of dead-man weight, liquid holdup and dynamic pressure of

particle flow. The dynamic pressure, which is caused by the particle converging flow within the active coke zone (cf. Fig .4), was assumed to decrease linearly along the radial dimension from the furnace center to the raceway front. The authors calculated the bottom profile of the dead man based on a simple pressure balance. It was found that the dead man floats higher beneath the raceways, showing that the distribution of the downward-acting pressure plays a crucial role in shaping the dead-man bottom. A more delicate estimation of the downward-acting pressure was presented by Takahashi et al. (2002), who classified the dead-man floating state into four categories, i.e., sitting, partly floating at the wall, completely floating with a flat bottom and completely floating, but floating higher near the wall. Nevertheless, most of the parameters used in the calculation of the downward-acting pressure are unknown in practice and have to be guessed, which makes the analysis results fairly speculative.

The radial distribution of the downward-acting pressure is, in fact, difficult to estimate and could vary in different furnaces and with the operating conditions. In order to judge if a (partly) floating dead-man state is possible, Brännbacka et al. (2003; 2004; 2005) formulated the downward-acting pressure (p_d) with a simple parameterized expression instead of attempting to precisely compute it.

$$p_\mathrm{d}(r) = \begin{cases} \bar{p}_\mathrm{d} & \text{if } r \le r_0 \\ \bar{p}_\mathrm{d} - a\left(\dfrac{r - r_0}{R}\right)^n & \text{if } r > r_0 \end{cases} \tag{1}$$

where $\bar{p}_\mathrm{d}$ is the overall pressure, r is the radial position, r_0 is the radius of the central region (cf. Fig. 4) where the downward-acting pressure is unaffected by the raceways and R, a are the scaling factor of length and pressure dimensions, respectively, while n is a parameter affecting the shape of the dead man bottom under the raceways. The magnitude of the overall pressure can be estimated by calculating the weight of the burden materials reduced by the lifting force of the upwards gas flow and supporting force of wall friction (Brännbacka and Saxén, 2003).

The vertical position of the dead-man bottom (z_{dm}) can thus be derived according to the force balance between the downward-acting pressure and buoyancy.

$$z_{dm} = \begin{cases} z_{sl} - \dfrac{p_d}{\rho_{sl} g(1-\varepsilon)} & \text{if } 0 \le p_d \le p_{b,sl}^{max} \\ z_{ir} + \dfrac{\rho_{sl}}{\rho_{ir}}(z_{sl} - z_{ir}) - \dfrac{p_d}{\rho_{ir} g(1-\varepsilon)} & \text{if } p_{b,sl}^{max} < p_d \le p_{b,sl}^{max} + p_{b,ir}^{max} \\ z_{hb} & \text{if } p_d > p_{b,sl}^{max} + p_{b,ir}^{max} \end{cases} \quad (2a)$$

$$p_{b,sl}^{max} = \rho_{sl} g(1-\varepsilon)(z_{sl} - z_{ir}); \; p_{b,ir}^{max} = \rho_{ir} g(1-\varepsilon)(z_{ir} - z_{hb}) \quad (2b, c)$$

where ρ_{ir}, ρ_{sl}, g and z_{hb} are the iron and slag densities, gravity and vertical level of the hearth bottom, respectively.

The dead-man profile was calculated by giving the liquids levels (z_{ir}, z_{sl}) and average dead-man porosity (ε). As can be seen in Fig. 5 (Brännbacka, 2004), the simple expression of downward-acting pressure is very flexible and is capable to shape the dead-man bottom in the hearth.

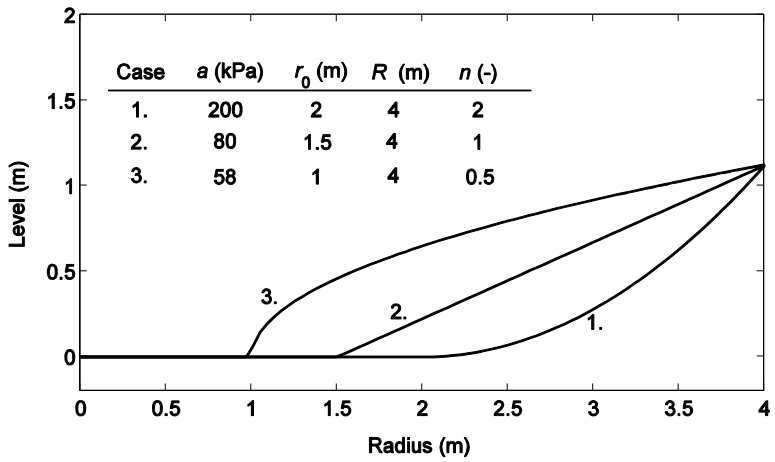

Figure 5. Resulting dead-man bottom profiles with some parameter values in Eq. (1) for a dead man with porosity of 0.35 (Brännbacka, 2004).

The dead-man bottom profile was also simulated by using DEM, as shown in Fig. 6, suggesting that the DEM simulation could approximately reproduce the internal dead-man structure observed in quenched Kurashiki No. 4 blast furnace (Nouchi et al., 2009). It is worth to note that the downward-acting pressure exerting on the top of the dead man was set to decrease as the wall was approached and the coke size was reduced due to the reaction with FeO in molten slag and carbon dissolution.

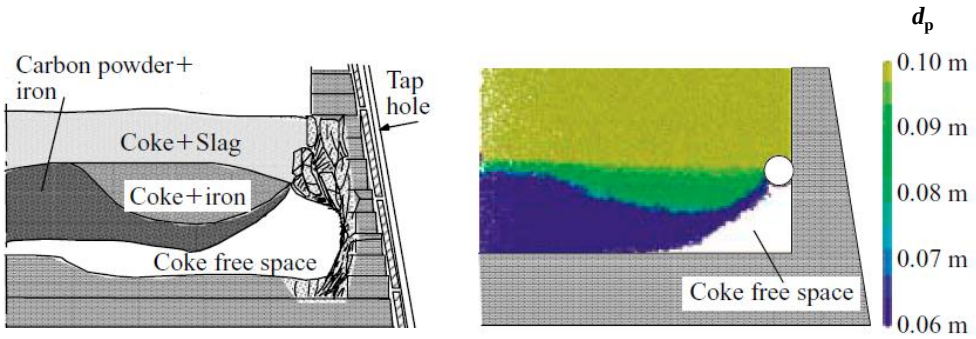

Figure 6. Internal structure of dead-man: (a) Dissection analysis of Kurashiki No. 4 blast furnace; (b) calculated result by Nouchi et al. (2009).

3.2 Lining condition of blast furnace hearth

The hearth is the central part of a blast furnace as the hearth condition significantly affects the whole furnace performance and determines the furnace campaign life. The development of furnace shaft repair techniques and improvement in operational control have enable campaign lives of over 15 years to be achieved without major outages (Jameson and Eden, 1999). However, the hearth, which is occupied by the molten liquids and unburned coke, cannot be repaired without a full stoppage of operation and extensive efforts. Severe damage of the hearth lining can even lead to catastrophic consequences and termination of the current campaign, which would cause huge losses of production and capital. The lining condition of the hearth is, therefore, of considerable importance for the extension of furnace campaign life.

3.2.1 Internal profile of blast furnace hearth

The hearth lining is eroded because of many reasons, such as chemical reactions between the refractory material and molten liquids, abrasion and friction due to unburned coke particles in the hearth, thermo-mechanical stress and flow induced shear stress (Vats and Dash, 2000). Since the sidewall and sometimes even the bottom of the hearth are cooled, the iron (possibly together with coke and other components) solidifies to form a skull layer on the (eroded) lining if the iron temperature and velocity are insufficient to keep iron in liquid form. As a result, the exact internal geometry of the hearth of an operating furnace is unknown.

The hearth internal profile has been studied through dissections of quenched furnaces and at the end of campaigns when the hearth is relined (Takeda et al., 1999; Inada et al., 1999, 2009; Nouchi et al., 2003). The reported hearth profile in such investigations is often "elephant-foot"-shaped with excessive lining erosion in the lower periphery of the hearth. This pattern is attributed to the intensive circumferential flows which probably emerge if the permeability in the center of the dead man deteriorates and/or the dead man partly floats, forming a free channel in the hearth corner. A bowl shaped profile, where the refractories in the middle portion of the hearth bottom are severely eroded, has also been found. This pattern could be expected if the dead man is fairly uniform and fills the whole hearth, or if the dead man floats completely with a fairly uniform height of the coke-free zone.

A completely sitting dead man with a low permeability zone in the bottom part to form a stable solidified layer was recommended as a method to extend the campaign life (Preuer and Winter, 1993). However, the dynamic behavior of the low permeability zone leads to wide variations in hearth temperature and tapped slag ratio (Takeda et al., 1999). In addition, too much cooling of the hearth bottom could solidify the lower part of a sitting dead man (inactive dead man), which is undesirable in furnace operation (Raipala, 2003). The common way of protecting the hearth lining from "elephant-foot"-shaped profile has been to increase the sump depth (i.e., the vertical distance from the taphole to the hearth bottom), which could ensure a fully floating dead man and thus considerably decrease the

flow velocities in the periphery region (Ohno et al., 1985; Vogelpoth et al., 1985; Shibata et al., 1991). Modern blast furnaces usually have a minimum sump depth of 20 % of the hearth diameter and this ratio still tends to increase in the design of new furnaces (Liu et al, 2012). Furthermore, the circumferential flow can be restrained if the liquids are drawn from the hearth center, which requires a long taphole and is facilitated by constructing the taphole buttresses at the beginning of the campaign (Jameson and Eden, 1999).

3.2.2 Modeling based on heat transfer and/or fluid flow

The blast furnaces usually have a large number of thermocouples embedded in the lining materials and these temperature measurements are applied to estimate the remaining thickness of the lining. The simplest and most commonly used technique has been based on solving the inverse heat transfer problem to predict the profile of the internal liquid-solid boundary (Torrkulla and Saxén, 2000; Kumar, 2005; Brännbacka and Saxén, 2008). The models were utilized to calculate the position of the 1150 ºC isotherm, which is usually regarded as the boundary between liquid iron and the hearth lining materials. It should be noted that these models were developed on the basis of certain assumptions and simplifications to make the problem manageable and possible to solve. Thus, the accuracy of the predicted hearth profile strongly depends on the model formulation and on the quality and quantity of the thermocouple readings available.

The liquid flow pattern inside the blast furnace hearth, which is intimately related to the hearth lining conditions, has been studied with both physical and numerical models. These investigations usually consider only iron phase and operate in steady-state, but the simulation results can still give valuable information about the liquid flow near the hearth bottom where the lining erosion is mainly caused by iron flows.

Several CFD models, taking into account liquid flow and/or heat transfer in blast furnace hearths, were developed in the past years (Shibata et al., 1990; Kowalski et al, 1998; Panjkovic et al., 2002; Guo et al., 2008). As a rule, the dead man was treated as a fixed packed bed where Darcy's/Ergun's equation is commonly applied. The effects of dead-man properties, such as floating state and packing structure, on the liquid flow pattern

and temperature profile in the lining refractories have been thoroughly assessed. The simulation results showed that a partly floating dead man gives rise to strong circumferential flow and thus imposes significant heat load on the lining at the hearth corner, and the circumferential flow is enhanced if the central porosity of the dead man is reduced. It was also reported that the circumferential flow can be restrained and the heat load at the sidewall in the vicinity of the taphole is effectively lowered with a longer taphole. This statement was confirmed in Kakogawa No. 2 blast furnace (Shibata et al., 1990). More recent results indicated that the temperature distribution at the hearth bottom is less sensitive to the dead man properties. Instead, it is controlled by the heat transfer across the lining refractories of the hearth (Guo et al., 2008).

The flow induced shear stress, which plays an important role in initiating and aggravating the hearth erosion along with other factors, has been given much attention in the recent decade (Vats and Dash, 2000; Dash et al., 2001, 2004). Since no direct measurements for the state variables in blast furnace hearths exist, CFD models have been established to carry out parametric studies. In these studies, both sitting and floating dead man were considered and the taphole was positioned inside an impermeable block which represents the “mushroom” of the solidified taphole clay in the real process. The simulation results showed that a peak shear stress appears in the azimuthal direction of the taphole during tapping operation and the peak shear stress becomes lower as the impermeable block is set longer, i.e., a longer taphole. It was also reported that there exist optimum values for the taphole length and inclination angle through which the shear stress exerted on the hearth sidewall is minimum.

3.3 Drainage behavior of blast furnace hearth

The drainage performance of iron and slag is important for the stable operation of the blast furnace as aforementioned. Failure to drain iron and slag effectively could result in high liquid levels within the hearth, which has adverse effects on furnace stability, productivity and efficiency. The situation becomes dangerous if the slag level rises excessively since the chemically aggressive slag may destroy the tuyeres and thus cause

water leakage into the molten liquids, which, in turn, can lead to explosion and endanger the casthouse personnel (Brännbacka, 2004).

3.3.1 Estimating slag residual ratio

To the best of our knowledge, the first attempt to deeply investigate the drainage behavior of the blast furnace hearth was made by Fukutake and Okabe (1976a), who conducted extensive experiments by using a physical cold model. The experimental results were analyzed based on fluid dynamics theories and a dimensionless flow-out coefficient was derived. It was found that the flow-out coefficient correlates monotonically with a slag residual ratio, defined as the ratio between the initial amount of slag and that remaining in the hearth at the tapping end (Fukutake and Okabe, 1976b). The experiments considered only the slag phase and assumed the slag-iron interface to be horizontal at the taphole level. This assumption was later proven to be erroneous because physical experiments and numerical simulations with two immiscible liquids revealed that iron phase could be drained to levels below the taphole (Tanzil et al., 1984; Tanzil and Pinczewski, 1987).

As slag flows towards the taphole through the dead man, its high viscosity gives rise to a substantial pressure drop near the taphole, which could elevate the slag-iron interface locally and allow iron to flow out even though the average slag-iron interface is below the taphole level. In order to consider the inclination of the slag-iron interface and a possible coke-free zone beneath the dead man, Zulli (1991) modified the flow-out coefficient proposed by Fukutake and Okabe. The experimental and numerical results both showed that the modified coefficient still correlates monotonically with a slag residual ratio, which was defined as the slag volume above the taphole at the end of the tap, relative to the initial slag volume above the taphole. The modified flow-out coefficient by Zulli is given as

$$F_L = 180\frac{(1-\varepsilon)^2}{\varepsilon^3}\frac{1}{{d_\mathrm{p}}^2}\frac{\mu_\mathrm{sl}}{\rho_\mathrm{sl}}\frac{U_0}{g}\left(\frac{D_\mathrm{h}}{z_{\mathrm{sl},0}}\right)^{1.4} \tag{3}$$

where ε is the dead-man porosity, d_p is the (effective) coke diameter, μ and ρ are the viscosity and density, U_0 is the mean superficial velocity, g is the gravitational acceleration, D_h is the hearth diameter, z is the vertical level, and the subscripts "sl" denotes slag. In addition, $z_{sl,0}$ is the initial slag level relative to the taphole level.

It should be pointed out that the physical aforementioned experiments were conducted with a constant outflow rate, which is only an extreme case of the real process. In fact, as the taphole is eroded the liquid drainage rate could increase during tapping. Bean (2008) further extended the flow-out coefficient modified by Zulli to account for the variation of drainage rate, continuous production of liquid, and taphole height, z_{th} (i.e., the sump depth), yielding

$$F_L^{*} = 180\frac{(1-\varepsilon)^2}{\varepsilon^3}\frac{1}{d_p^{\,2}}\frac{\mu_{sl}}{\rho_{sl}}\frac{U_e}{g}\left(\frac{D_h}{z_{sl,0}+z_{prod}}\right)^{2Ri} \tag{4a}$$

where U_e is the mean superficial velocity at the end of the tap, z_{prod} is the equivalent level corresponding to the slag production during the tap. The exponent is given as

$$Ri = \left(1-1.5Rh+1.46Rh^2-0.46Rh^3\right)^{1/3}; \qquad Rh = \frac{z_{sl,0}}{z_{th}} \tag{4b, c}$$

Also, the slag residual ratio was correspondingly redefined as

$$\alpha = \frac{V_e}{V_0+V_{prod}} \tag{5}$$

where V_e is the slag volume above the taphole at the end of the tap, V_0 is the initial slag volume above the taphole and V_{prod} is the volume of slag produced (i.e., entering the hearth) during the tap.

Both physical experiments and numerical simulations have shown that the most important factors increasing the residual amount of slag are low dead-man permeability, high liquid

viscosity and drainage rate (Fukutake and Okabe, 1976 a; Tanzil et al., 1984; Zulli, 1991; Nishioka et al., 2005a, b). In the case of a dead man with inhomogeneous permeability, it is far more complicated to predict the tap end since the viscous fingering may cause gas to burst out prematurely (Zulli et al., 2003; He et al., 2006). In addition, the coke-free zones affect the drainage behavior considerably only if they extend close to or above the taphole level (Zulli, 1991; Nouchi et al., 2003; Nishioka et al., 2005b).

3.3.2 Asymptotic relationship between liquid levels at tapping end

The liquid level at the end of a tap is an important factor in blast furnace operation since it gives information about the dead-man properties especially in front of the taphole. The tap-end liquid levels also affect the maximum slag level during the following tap and therefore, the next drainage strategy. The relationship between iron and slag levels at the tap end can be described by a simplified pressure balance, as schematically illustrated in Fig. 7 (Tanzil et al., 1984).

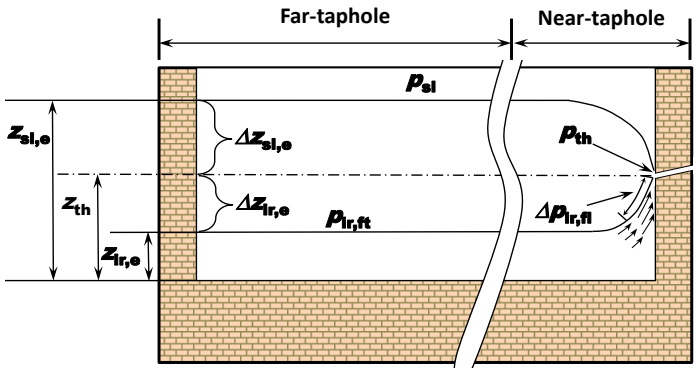

Figure 7. Schematic of iron and slag levels at the end of a tap.

In the far-taphole region (cf. Fig. 7), iron and slag levels can be assumed to be horizontal and the dynamic pressure gradients caused by liquid flows are negligible due to low flow rates. The pressure at the overall slag surface is therefore assumed to be constant, equaling the taphole pressure since the slag surface declines down to the taphole at the end of the tap, i.e., $p_{sl} = p_{th}$. The pressure difference between the liquid surfaces in the far-taphole region is given as

$$p_{\mathrm{ir,ft}} - p_{\mathrm{sl}} = \rho_{\mathrm{sl}} g \left(\Delta z_{\mathrm{sl,e}} + \Delta z_{\mathrm{ir,e}} \right) \tag{6a}$$

$$\Delta z_{\mathrm{sl,e}} = z_{\mathrm{sl,e}} - z_{\mathrm{th}} \; ; \; \Delta z_{\mathrm{ir,e}} = z_{\mathrm{th}} - z_{\mathrm{ir,e}} \tag{6b, c}$$

where the subscripts “ir”, “ft” and “e” stand for iron, far-taphole region and tapping end, respectively.

The pressure difference at the iron surface between far-taphole region and taphole can be expressed as

$$p_{\mathrm{ir,ft}} - p_{\mathrm{th}} = \rho_{\mathrm{ir}} g \, \Delta z_{\mathrm{ir,e}} + \Delta p_{\mathrm{ir,fl}} \tag{7}$$

where $\Delta p_{\mathrm{ir,fl}}$ is the dynamic pressure drop caused by iron flow near the taphole.

Inserting $p_{\mathrm{th}} = p_{\mathrm{sl}}$ and combining Eqs. (6a) and (7) yield

$$\Delta z_{\mathrm{ir,e}} = \frac{\rho_{\mathrm{sl}}}{\rho_{\mathrm{ir}} - \rho_{\mathrm{sl}}} \Delta z_{\mathrm{sl,e}} - \frac{\Delta p_{\mathrm{ir,fl}}}{\left(\rho_{\mathrm{ir}} - \rho_{\mathrm{sl}} \right) g} \tag{8}$$

In Eq. (8), the pressure drop due to iron outflow, $\Delta p_{\mathrm{ir,fl}}$, is not known and cannot be easily estimated in practice. Nevertheless, it is easy to see that this term is always positive if there is an iron outflow. Therefore, setting $\Delta p_{\mathrm{ir,fl}} = 0$ gives an absolute asymptotic limit for the iron level below which no iron can be drained (Tanzil et al., 1984).

$$\frac{\Delta z_{\mathrm{ir,e}}}{\Delta z_{\mathrm{sl,e}}} = \frac{\rho_{\mathrm{sl}}}{\rho_{\mathrm{ir}} - \rho_{\mathrm{sl}}} \tag{9}$$

3.3.3 Estimating liquid levels and drainage rates

As there are no practical means to directly measure the liquid levels in blast furnace hearth, the most common method is based on a mass balance analysis: If the instantaneous production and drainage rates of iron and slag are considered in a material

balance, changes of liquid volume in the hearth can thus be determined, if the liquid densities are known. The volume changes, in turn, can be transformed into liquid level variations if the dead-man properties such as porosity and floating state, and the inner profile of the hearth are "known". However, it is usually nontrivial to derive these variables from real process data and this step may require thorough modeling and investigations of the hearth conditions (Brännbacka, 2004).

The lack of instantaneous liquid drainage rates was earlier one of the main obstacles for a successful application of the mass balance model. An obvious way of estimating the instantaneous drainage rates is to directly weigh the tapped materials with a small time interval during tapping. Moreover, some more advanced methods have been reported and been implemented in several plants: Iron drainage rate can be calculated from the level variation in a hot metal ladle or torpedo; slag drainage rate can be estimated by monitoring the power requirement of the granulation drum or the heat transfer to the cooling water in the granulation unit. Nevertheless, these methods are strongly sensitive to measurement uncertainties and errors. For example, errors in the iron drainage rate could be considerable even for a single ladle due to inaccuracies in estimating the ladle geometry, which varies because of lining erosion or skull formation (Brännbacka and Saxén, 2001).

Alternatively, the outflow rates of iron and slag can be estimated on the basis of a pressure balance. The pressure difference between the tuyeres level and the outlet of the taphole (i.e., atmosphere) balances the resistances induced by liquid flows through the dead man and taphole. A comprehensive CFD model was developed by Nishioka et al. (2005a, b) to predict the slag residual ratio and drainage rates of iron and slag for industrial furnaces. In particular, the effect of the pressure drop caused by the taphole flow was taken into account by subtracting a term given by a simple expression from the total in-furnace pressure in every computational time-step. A similar treatment was later adopted by Iida et al. (2008, 2009), who studied the deviations of tapping time (or liquid drainage rates) under different operation conditions and hearth states. Based on the pressure balance in the furnace hearth, the drainage rates of iron and slag, which are

implicitly contained in the pressure drop expressions of flows in the coke-particle bed (dead man) and the taphole, were iteratively computed.

The problem with the this treatment is that the expression employed to calculate the pressure drop essentially assumes that iron and slag be perfectly mixed and that fully dispersed two-phase flow occurs in the taphole. As a result, the average liquid quantities, i.e., density and viscosity, were applied. In practice, there exist no direct ways to measure or observe the taphole flow due to the hostile conditions with high temperature and chemically aggressive liquids. The assumption of fully dispersed flow in the taphole is presumably made by considering the high drainage rates and the small taphole size compared to the hearth dimensions or simply as an approximation. Nevertheless, the use of an average viscosity of two immiscible liquids can be questioned and the large density difference between iron and slag would make it more natural to assume separated flow in the taphole.

To the best of our knowledge, the only two-phase flow studies of blast furnace taphole were focused on the simultaneous flow of gas and liquid, i.e., iron (He et al., 2002; Stevenson and He, 2005). The authors noted that a splashy taphole stream can increase the consumption of trough refractories and thus affect the total operation costs. They carried out physical modeling on the basis of geometric and dynamic similarities, and concluded that the occurrence of gas entrainment in the liquid, i.e., dispersed flow of gas and liquid in the taphole, is the root cause. The experimental results also showed that the dispersed flow takes place when the gas/liquid flow rate ratio exceeds a specific threshold and the packed bed (i.e., dead man) in the vicinity of the taphole acts as a buffer medium and only delays the occurrence of the dispersed flow. From a theoretical standpoint, such a gas-liquid system represents a very particular extreme that makes it easier to be dispersed compared to the liquid-liquid (e.g., slag-iron) system. However, even for this gas-liquid system, the authors pointed out that slug flow (i.e., not fully dispersed flow) is more likely to occur in the taphole under typical operation conditions of the blast furnace studied.

3.4 Conclusions

The liquid flows in blast furnace hearth and the associated erosion state have been simulated and predicted by using different CFD models on the basis of comparable cases (e.g., experimental model runs) where the internal conditions of the hearth are known. However, the internal conditions inside a real blast furnace hearth, to a large extent, are unknown, which makes setting up the geometry and boundary conditions a very complicated process. It is therefore necessary to estimate the pertinent (boundary) conditions, such as liquid level and dead man state before conducting the CFD work. Furthermore, the significance of taphole conditions on the blast furnace operation has been stressed in several reports. Various strategies for taphole management to control the hearth performance and furnace operation have been also recommended and already applied in some plants. However, the knowledge about the taphole flows of iron and slag is still very limited.

The research work summarized in this thesis concentrates on solving some of the problems mentioned above. A set of models for estimating the hearth drainage behavior and taphole flow patterns were developed and are described in the following chapter.

Chapter 4
Models Developed in this Thesis

The papers included as appendices in the thesis (as reported in "*Contribution of the author and list of publications*") are listed in a "self-correcting" order and the focus of each paper is schematically indicated in Fig. 8. **Paper I** presents a CFD model with the aim to deepen the understanding of iron flow and refractory erosion on the hearth bottom. The key boundary conditions of the CFD model are estimated by using a drainage model based on pressure balance analysis. By examining the correlation between the iron outflow trend and the taphole diameter from an industrial blast furnace, an advanced drainage model is proposed in **Paper II** in order to consider the effects of taphole conditions on the hearth performance. The taphole flows are further studied in **Papers III** and **IV**, where different models are developed to both simulate and predict the two-liquid flow patterns in the taphole. **Paper V** presents an integrated tap cycle model on the basis of simple material balance in the hearth and the assumption of fully stratified flow in the taphole. Finally, an improved CFD model that is able to take into account the interfacial forces between immiscible liquids (e.g., iron and slag) is presented and evaluated in **Paper VI**.

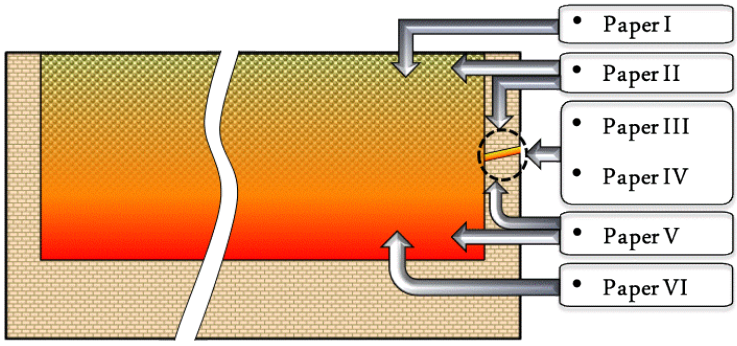

Figure 8. Focus of the papers appended to this thesis.

In the forthcoming text, the above papers are referred to as Paper I – Paper VI and the models and results of the papers are reported and discussed in detail in this chapter. Some of the models were developed for and evaluated on short-term data from a commercial blast furnace with only one taphole. In general, the furnace is tapped 12 times daily and produces approximately 3500 metric tons of hot metal per day. The outflow rates of iron and slag during tapping are measured (with a 5-minute interval) by utilizing different techniques (Brännbacka, 2004).

For the blast furnace studied, a typical tap cycle usually starts as the previous tap is finished and the taphole is plugged with clay (at $t_e(k\text{-}1)$, as depicted in Fig. 9) to let iron and slag accumulate in the hearth. When the taphole is drilled open at $t_0(k)$, iron often starts flowing out first because its level has risen above the taphole during the plugging period (inter-tap period Δt_{pl}). Slag will not be drained until the iron level descends to the vicinity of the taphole, leading to a slag delay, Δt_{sd}. After this moment (t_{ss}), iron and slag are drained simultaneously until gas bursts out, and finally, taphole plugging ends the current tap cycle at $t_e(k)$, even though the average slag level is still well above the taphole.

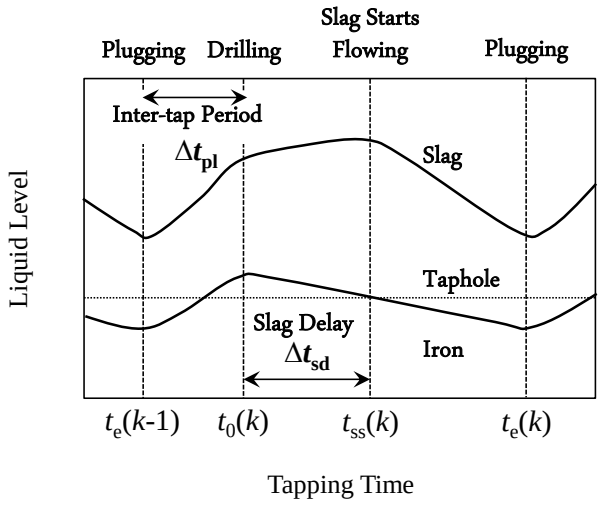

Figure 9. Schematic illustration of liquid levels during a typical tap cycle, numbered *k*.

4.1 Drainage model based on pressure balance analysis

A model estimating the dead-man state and liquid levels of the (one-taphole) blast furnace hearth was developed by Brännbacka and Saxén (2003). The model is based on a balance analysis between the downward-acting force and buoyancy force exerted on the dead man. By giving specific parameters, such as dead-man porosity, hearth geometry and liquid in- and outflow rates, the evolutions of liquid levels (cf. Fig. 9) as well as dead-man state during tapping can be simulated. In Paper I, this model was slightly improved by considering the relationship between tap-end levels of iron and slag, cf. Eq. (8).

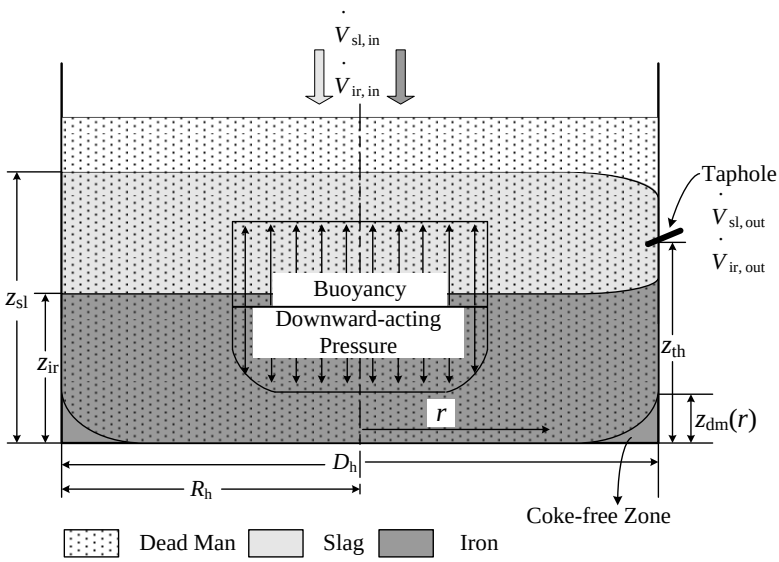

Figure 10. Illustration of drainage model based on a pressure balance

4.1.1 Coupling of liquid levels and volumes

The main concepts of the drainage model, as well as the pertinent notation, are illustrated in Fig. 10. At a certain point of the tapping duration, when iron and slag levels are known, the dead-man bottom profile can be calculated according to Eqs. (1) and (2). The volume of coke-free zone is thus computed by

$$V_{\mathrm{cf}} = 2\pi \int_0^{R_{\mathrm{h}}} z_{\mathrm{dm}} r \, \mathrm{d}r \tag{10}$$

It should be noted that if the buoyancy is insufficient to overcome the downward-acting force (cf. Eqs. (1) and (2)), the dead man will sit at the hearth bottom giving $V_{\mathrm{cf}} = 0$.

The time-dependent in- and outflow rates give the instantaneous liquid volumes in the hearth by

$$V_{\mathrm{i}} = V_{\mathrm{i},0} + \int_0^t \dot{V}_{\mathrm{i,in}} \mathrm{d}t - \int_0^t \dot{V}_{\mathrm{i,out}} \mathrm{d}t, \qquad i = \{\mathrm{ir, sl}\} \tag{11}$$

where V_0 is the initial liquid volume at the moment when the taphole is drilled open, and t is the tapping time.

The relationship between liquid level and volume is complicated, in particular for the case where the dead man (partly) floats, leading to a coke-free zone at the hearth bottom. By assuming that the coke-free zone never extends to the taphole level, the volume-level coupling can be given as a general expression

$$\frac{\mathrm{d}z_{\mathrm{i}}}{\mathrm{d}V_{\mathrm{j}}} = \frac{1}{A\varepsilon}\left(\sigma - (1-\varepsilon)\frac{\mathrm{d}V_{\mathrm{cf}}}{\mathrm{d}V_{\mathrm{j}}}\right), \quad j = \{\mathrm{ir, sl}\} \tag{12}$$

where $\sigma = 0$ if i = ir and j = sl, otherwise $\sigma = 1$; A is the hearth cross-sectional area; dz, dV and dV_{cf} are the variations in liquid level, liquid volume and coke-free volume, respectively.

4.1.2 Case studies

Seven cases were studied with the drainage model in Paper I to assess the effects of production rate, downward-acting pressure, dead-man porosity and sump depth/taphole height on the drainage behavior, as listed in Table 2.

The first row of Table 2 reports the base case (Case 1) with a sitting dead man, which was realized by imposing a sufficient downward-acting pressure, $\bar{p}_{\mathrm{d}}$, in Eq. (1) to prevent the dead man from floating (i.e., 150 kPa), while $\bar{p}_{\mathrm{d}}$ was set lower for the remaining cases in the table to study the effect of a floating dead man. The evolutions of liquid levels for Case 1 and Case 2 are illustrated in Fig. 11, where the liquid levels are seen to vary on a lower level when the dead man is (partly) floating (cf. dashed lines in the figure). This is caused by the emergence of the coke-free zone, as shown in Fig. 12.

Table 2. Effects of iron production rate, downward-acting pressure, dead-man porosity and taphole height on the outflow levels of slag and iron, outflow volume of coke-free zone. States denoted by S, PF and FF correspond to sitting, partly floating and fully floating, respectively.

Case	Production [t/d]	$\bar{p}_{\mathrm{d}}$ [kPa]	ε [-]	z_{th} [m]	$z_{\mathrm{sl},0}$ [m]	$z_{\mathrm{ir},0}$ [m]	$V_{\mathrm{cf},0}$ [m^3]	State
1.	3400	150	0.35	1.5	**3.11**	**1.96**	**0**	**S**
2.	3400	**110**	0.35	1.5	**2.82**	**1.73**	**5.41**	**PF**
3.	3400	**110**	0.35	**2.1**	**3.22**	**2.13**	**13.66**	**FF**
4.	**3200**	**110**	0.35	1.5	**2.75**	**1.72**	**4.94**	**PF**
5.	**3600**	**110**	0.35	1.5	**2.89**	**1.74**	**5.89**	**PF**
6.	3400	**110**	**0.30**	1.5	**2.93**	**1.63**	**7.38**	**PF**
7.	3400	**110**	**0.40**	1.5	**2.74**	**1.79**	**3.55**	**PF**

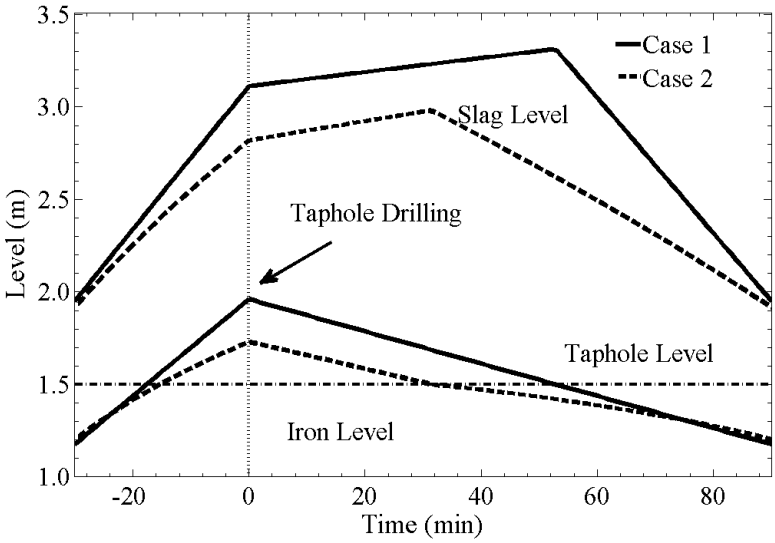

Figure 11. Evolutions of liquid levels for Case 1 (solid lines) and Case 2 (dashed lines) in Table 2.

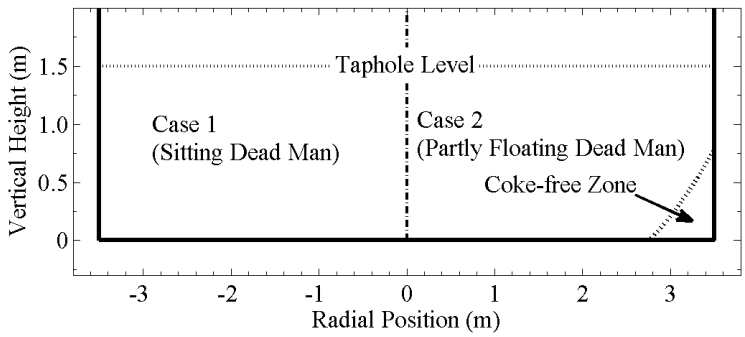

Figure 12. Hearth geometries and dead-man positions of Case 1 and Case 2 in Table 2.

A fully floating dead man is obtained in Case 3, where the taphole height (i.e., sump depth) of the hearth was increased to 2.1 m. The local state of the fully floating dead man is plotted in Fig. 13, where it is found that the horizontal bottom of the dead man is only about 1 cm above the hearth bottom. It is surprisingly small compared to what were assumed by other researchers. However, due to the dead-man shape near the hearth sidewall the case still corresponds to a large coke-free zone (cf. Table 2).

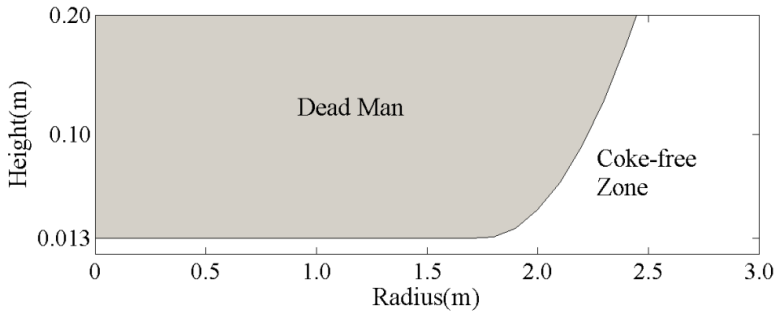

Figure 13. Local state of the fully floating dead man of Case 3 in Table 2.

4.2 Estimating iron flow and hearth erosion

The iron flow and hearth erosion caused by flow-induced shear stress have been investigated by developing an integrated CFD model. The liquid flow in the blast furnace hearth is typically complicated and does not appear in a single flow regime: The molten liquids are in LRN (Low-Reynolds Number) regime as they dribble into the hearth, whereas they gradually accelerate as they approach the taphole, resulting in HRN (High-Reynolds Number) flows in the vicinity of the taphole. Moreover, the flow velocity increases in the local coke-free zones due to a sudden decrease in flow resistance. A modified k-ω turbulence model was adopted in Paper I to account for these complicated turbulent features.

4.2.1 Key boundary conditions

In the real process, iron flow in the hearth is affected by a number of operating conditions such as sump depth, taphole length, dead-man porosity, coke diameter, outflow rates and dead-man floating state. Here, some of these parameters are directly given as inputs to the CFD model except for two key boundary conditions, i.e., dead-man floating state and iron level (i.e., inlet height of the computational domain).

The CFD model was implemented in ANSYS FLUENT. The top inlet height was given by the calculated iron level, which is reported in Table 2. The dead-man state, including its shape and position, was reconstructed in a numerical way. The three types of the dead-

man configuration, i.e., sitting, partly floating and fully floating were treated by a general User Defined Function (UDF), which can considerably reduce the efforts for geometry creation and mesh generation.

Figure 14 shows the dead-man cross-sectional profile of Case 2 (cf. Table 2) before and after the UDF implementation. The solid-liquid interface (smooth curve in the upper panel of the figure) is represented by a zigzag line (in the lower panel) which is made up of edges of numerous discretized cells.

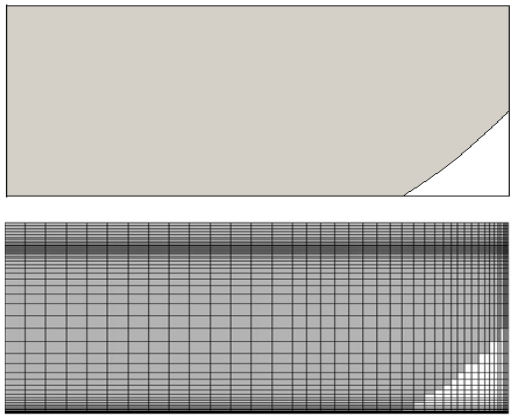

Figure 14. Dead man cross-sectional profile of Case 2 (gray: dead man, white: coke-free zone). Upper panel: mathematical solution with the drainage model. Lower panel: numerical reconstruction with UDF.

4.2.2 Results

According to Guo et al. (2006), the flow regime in a packed bed (e.g., the dead man in the hearth) can be determined by the pore Reynolds number, $Re_p = \varepsilon \rho_{ir} |\mathbf{u}| d_p / \mu_{ir}$, with (unsteady) laminar flow for $Re_p < 300$ and fully-developed turbulent flow for $Re_p \geq 300$. For the cases listed in Table 2, it was found that fully-developed turbulent regions occur both close to the taphole and in the coke-free zone (only for the cases with floating dead man). However, the volume of the fully-developed turbulent region(s) is small compared to the whole hearth domain.

The fully-developed turbulent regions for Case 2 with a partly floating dead man are illustrated in Fig. 15. The results imply that the standard *k-e* turbulence model, which was initially proposed for a regime that is dominated by fully-developed turbulent flow, could not be proper for describing the flow in the blast furnace hearth.

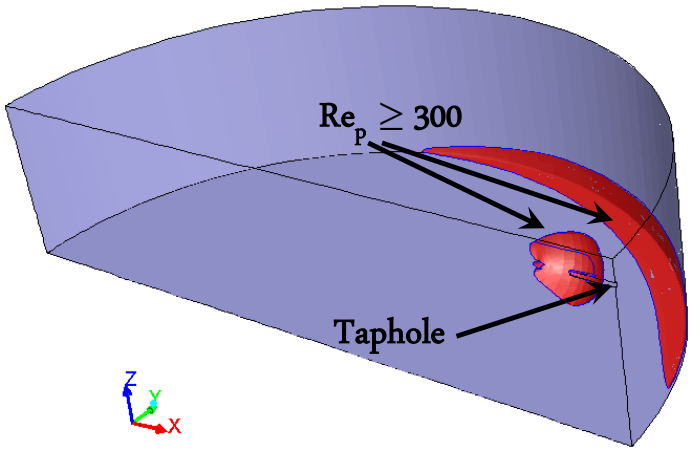

Figure 15. Illustration of fully-developed turbulent regions ($Re_p \geq 300$) for Case 2 in Table 2.

Figure 16 displays the streamlines of Case 2 with a partly floating dead man. By comparing this with the result for a sitting dead man (Case 1 in Table 2), it was found that the streamlines are almost identical when the injection distance, denoted by "*l*" in the figure, is less than a critical value regardless of the dead-man floating state. However, as the injection distance exceeds the critical value, iron tends to take the peripheral path (i.e., coke-free zone) formed beneath the dead man, leading to the circumferential flows at hearth corner.

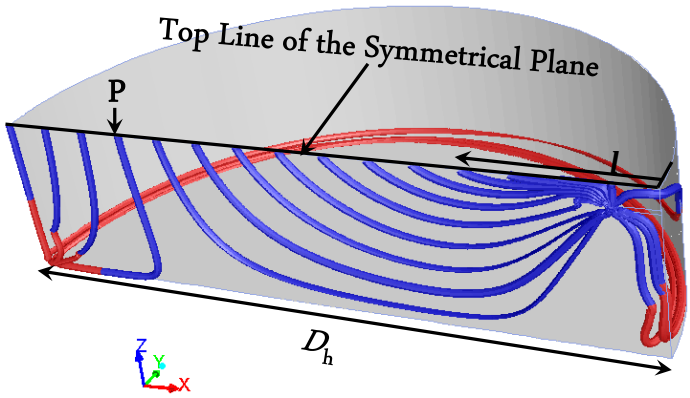

Figure 16. Streamlines in the hearth with a partly float dead man (Case 2). Blue sections: flow through the dead man. Red sections: flow through the coke-free zone.

The contours of shear stress on the hearth bottom are shown in the left panel of Fig. 17. With a sitting dead man, the high shear-stress zone appears in the interior of the hearth bottom, particularly below the taphole entrance. However, this zone shifts to the peripheral region if the coke-free zone emerges, i.e., Cases 2 and 3 in the figure.

The effect of dead-man floating state on the shear stress is further investigated in the right panel of Fig. 17, where the normalized shear stress along the orthogonal line at the hearth bottom (cf. dashed line in the top left panel) is plotted. For a sitting dead man, the shear stress is seen to monotonously decrease along the radial direction of the hearth bottom, which could give rise to a bowl shaped erosion profile because the central part of the bottom lining suffers stronger wear of shear stress. By contrast, the shear stress is found to be higher at the hearth corner if the dead man either partly or fully floats, which could lead to an “elephant-foot”-shaped erosion pattern.

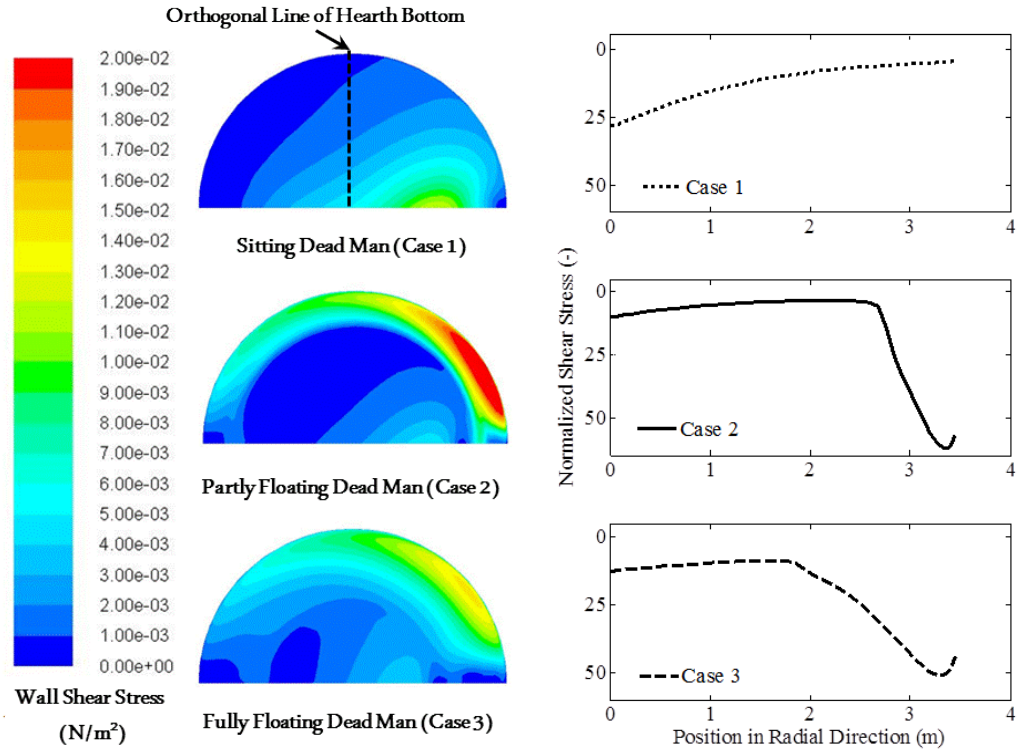

Figure 17. Left: Contours of shear stress on the hearth bottom for different dead-man states. Right: Normalized shear stress along the orthogonal line on the hearth bottom for different dead-man states.

4.3 Advanced drainage model

In the first drainage model presented in subsection 4.1, a very simplified approach for describing the outflow patterns of iron and slag was used: Slag is assumed to flow out in a constant rate when the slag-iron interface has descended to the taphole and the drainage rate of iron is constant during the whole tap even after slag has started draining. To make the description more realistic and comprehensive, the assumption concerning outflow patterns of iron and slag was revised by considering the effects of taphole size and length. For a detailed description of the more advanced drainage model, the reader is referred to Paper II.

4.3.1 Case studies

The advanced drainage model was applied on fourteen cases in Paper II as listed in Table 3, where the changes from the base case (Case 1) and calculated results are boldfaced.

Table 3. Effects of iron production rate, downward-acting pressure, dead-man porosity, hearth diameter, taphole height, diameter and length on slag delay and coke-free volume (at slag outflow start). States denoted by S and F correspond to a sitting or (partly) floating dead man.

Case	$\dot{m}_{ir}$ [t/d]	$\bar{p}_d$ [kPa]	ε [-]	D_h [m]	z_{th} [m]	d_{th} [mm]	l_{th} [m]	Δt_{sd} [min]	$V_{cf,ss}$ [m^3]	State
1.	3400	150	0.35	7	1.5	39	2.1	**59**	**0**	**S**
2.	**3100**	150	0.35	7	1.5	39	2.1	**55**	**0**	**S**
3.	3400	150	**0.25**	7	1.5	39	2.1	**51**	**0**	**S**
4.	3400	150	0.35	**8**	1.5	39	2.1	**58**	**0**	**S**
5.	3400	150	0.35	7	**2.0**	39	2.1	**61**	**0**	**S**
6.	3400	150	0.35	7	1.5	**42**	2.1	**48**	**0**	**S**
7.	3400	150	0.35	7	1.5	39	**1.6**	**52**	**0**	**S**
8.	3400	**130**	0.35	7	1.5	39	2.1	**59**	**0.19**	**S/F**
9.	3400	**110**	0.35	7	1.5	39	2.1	**49**	**2.82**	**F**
10.	3400	110	**0.25**	7	1.5	39	2.1	**14**	**7.56**	**F**
11.	3400	110	0.35	**8**	1.5	39	2.1	**42**	**4.42**	**F**
12.	3400	110	0.35	7	**2.0**	39	2.1	**23**	**8.30**	**F**
13.	3400	110	0.35	7	1.5	**42**	2.1	**39**	**2.03**	**F**
14.	3400	110	0.35	7	1.5	39	**1.6**	**43**	**2.28**	**F**

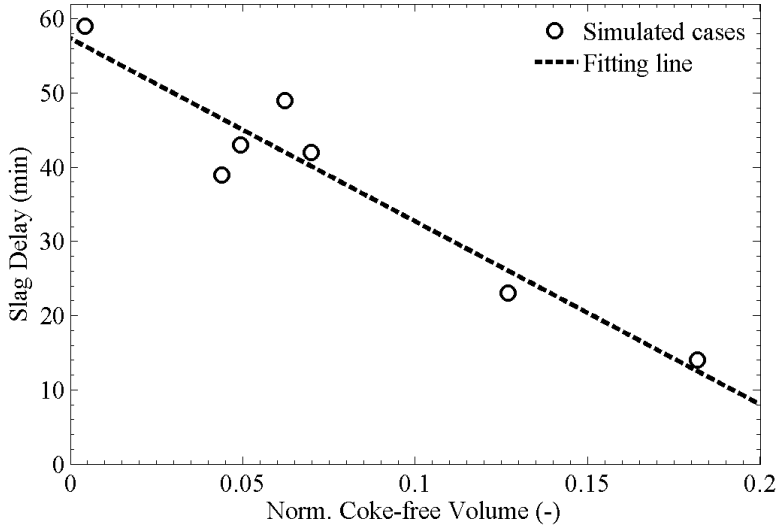

Figure 18. Relation between normalized coke-free volume and slag delay for the cases with floating dead man (cf. Table 3).

The upper part of Table 3 illustrates a set of cases with sitting dead man, which is realized by giving $\overline{p}_{\mathrm{d}}$ a high value. It was found that the changes in slag delay are relatively small compared to the quite drastic variations in the input conditions. Case 8 with a lower $\overline{p}_{\mathrm{d}}$ corresponds to a transitional state, where the dead man barely floats and the coke-free volume is very small. The dead man becomes floating as $\overline{p}_{\mathrm{d}}$ is further reduced, and the drainage behavior in terms of slag delay becomes completely different, as shown in the lower part of Table 3. Figure 18 displays the dependence between the coke-free volume ($V_{\mathrm{cf,ss}}$) and slag delay for the cases with floating dead man. To allow for better comparison, the coke-free volume was normalized by the sump volume below the taphole level. A strong negative and rather linear correlation between the two variables is observed, also showing very good agreement with results obtained on analysis of long-term process data (Brännbacka, 2004).

4.3.2 Estimating dead-man porosity

To assess its validity, the advanced drainage model was evaluated throughout a 20-day period data from the blast furnace studied. For this short period, the dead-man porosity

and coke size were given average values of 0.3 and 0.035 m, respectively. The calculation was based on daily averages of iron and slag production, tapping strategy (taphole plugged time, tap length, taphole diameter) and taphole length. Measured (asterisks) and simulated (solid line) slag delays are depicted in Fig. 19, showing that the advanced model can capture the main trend shown by the slag delay during the short period. However, some small discrepancies between the observed and simulated results exist.

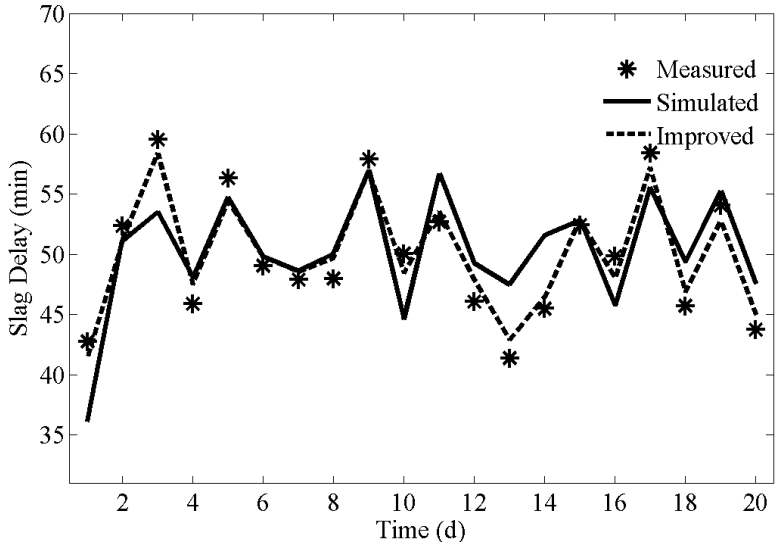

Figure 19. Comparison of measured and simulated slag delays over a 20-day period of the industrial blast furnace.

In order to explain the small discrepancies, the dead-man porosity was adjusted on the basis of the measured slag delay (Δt_{sd}^{*}) using a simplified scheme, cf. Paper II. The improved results, also displayed in Fig. 19 with dashed line, exhibit very good agreement with the process data, which is quite natural since the dead-man porosity was allowed to vary. The relation between the adjusted porosity and specific slag ratio from the process data is shown in Fig. 20, in which the corresponding operation date is also reported with small circles. A positive correlation between the variables (cf. the dashed fitting line) can be seen and it is interesting to note the estimated short-term variation in dead-man porosity and the decreasing trend from “A” to “B” in the figure. Such changes in dead-

man porosity were reported (Nightingale and Tanzil, 1997) and may be due to the changes in the quality of the charged coke.

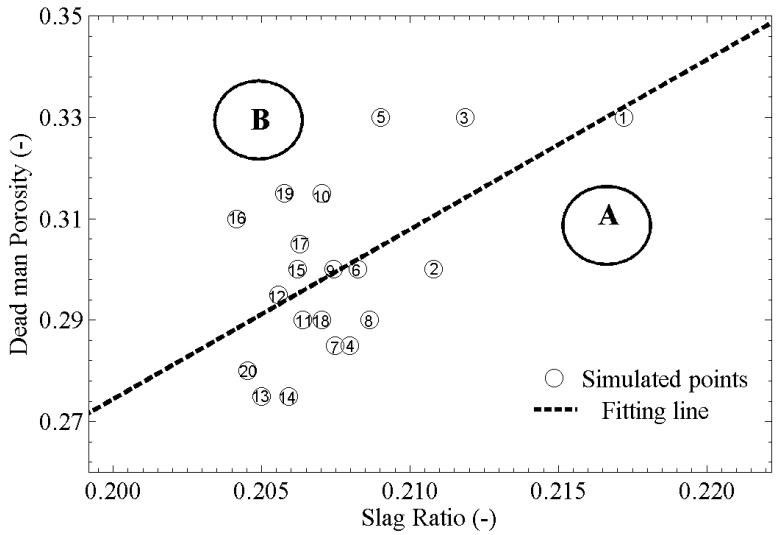

Figure 20. Relation between calculated dead-man porosity and slag ratio.

4.4 Iron and slag flow in taphole

The flow of molten iron and slag in the blast furnace taphole has not been received much attention in the literature even though it has been stressed to have great influence on the hearth drainage performance. Some characteristic features of the two-liquid flow in the taphole of the reference furnace were investigated in Paper III and Paper IV by using a set of analysis models and techniques.

4.4.1 Slag-iron interface in taphole

In Paper III the transient flow behavior of iron and slag in the taphole was simulated by applying a VOF (Volume Of Fluid) -based CFD model, where the hearth was idealized as a finite-volume liquid reservoir to generate appropriate inlet conditions for the taphole flow and thus considerably alleviate the computational burden because the entire hearth dimensions are big compared to the taphole size. The computational domain and relevant

boundary conditions are shown in Fig. 21, where only half of the volume is plotted because of symmetry. The taphole length (l_{th}) and height (z_{th}) are also depicted in the figure. The taphole is located at a small distance above the bottom of the liquid reservoir ($z_{th} = 3d_{th}$) because the main focus was put on the flow conditions near the taphole. Slag was taken into the liquid reservoir by a mass flow rate ($\dot{m}_{sl,in}$) corresponding to the daily production of the reference furnace and atmospheric pressure was set at the taphole outlet.

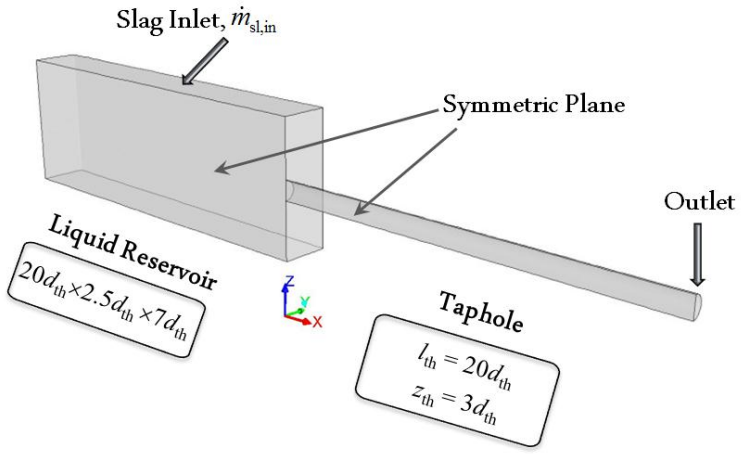

Figure 21. Computational domain and boundary conditions.

A short-term tap was performed by iterative calculations until t = 10.0 s. Based on the simulation results, the taphole flow can be concluded to follow two different patterns during tapping: At the intermediate stage (here t = 2.0-5.0 s) of the tap, iron and slag flow through their respective channels with no obvious phase dispersion; only small slugs and droplets are observed. This pattern is called separated flow. For the rest of the tapping stages, the interface in the taphole is very wavy and phase dispersion commonly occurs, so the flow is (partially) dispersed.

Dispersed flow

The dispersed flow patterns at two points at times t = 1.0 s and t = 10.0 s are illustrated in Fig. 22, where half of the taphole is plotted. At t = 1.0 s (upper panel), iron is the primary phase flowing through the taphole and slag is drained in a narrow channel above the iron,

where some slugs and droplets of iron can be found. This is mainly caused by the large difference in the liquid flow rates and volume fractions: The slag phase with lower flow rate and volume fraction competes with iron for its share of the taphole, giving rise to phase inversion in the slag channel. Similarly, the dispersions of slag phase in the iron channel can take place when slag becomes the primary phase at t = 10.0 s (lower panel).

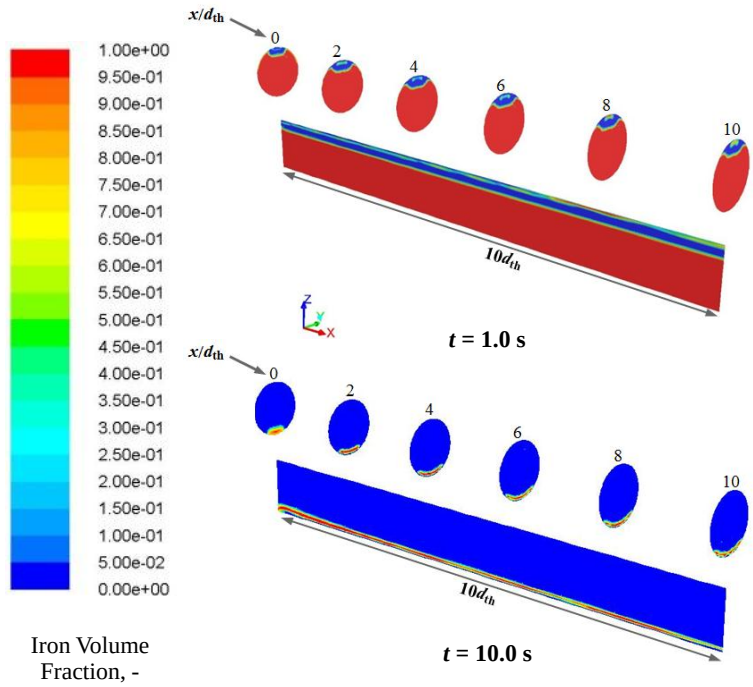

Figure 22. Dispersed flows at early (top) and late (bottom) stages of the tap.

Separated flow

The separated flow patterns (observed at t = 2.0-5.0 s) are displayed in Fig. 23, where slag-iron interfaces are well-defined and no obvious dispersions can be observed in the taphole. This could be explained by the comparable liquid flow rates and volume fractions: None of the two phases could become dominant in the taphole and the large density difference can decay small fluctuations at the interface to some degree.

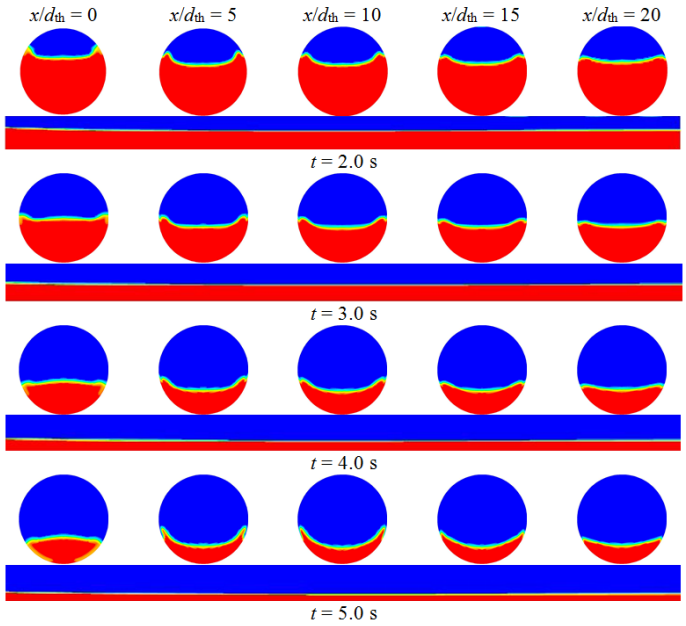

Figure 23. Separated flows in the taphole.

4.4.2 Prediction of slag-iron flow pattern in taphole

Paper III revealed that separated flow can be dominant if the outflow rates of iron and slag are comparable during tapping. The taphole flow patterns were further predicted with a well-developed Zero Real Characteristic (ZRC) model (Brauner and Maron, 1992a, b) in Paper IV. The ZRC model was applied to the process data of four different taps from the reference furnace, as shown in Fig. 24.

The predicted flow patterns for the four taps are depicted in Fig. 25, where the calculated ZRC criterion for all combinations of the measured liquid flow rates is plotted. Both the ZRC criterion and the tapping time were normalized to make it possible to plot the results in one figure. It can be seen that most C_{zrc} values are positive, which implies that the taphole flow is separated. The reasons for some of the points showing negative C_{zrc} values indicating dispersed flow are the large occasionally appearing sudden decreases in the liquid flow rates (cf. Fig. 24), where possibly loose coke particles temporary choke the taphole during tapping (Brännbacka and Saxén, 2001).

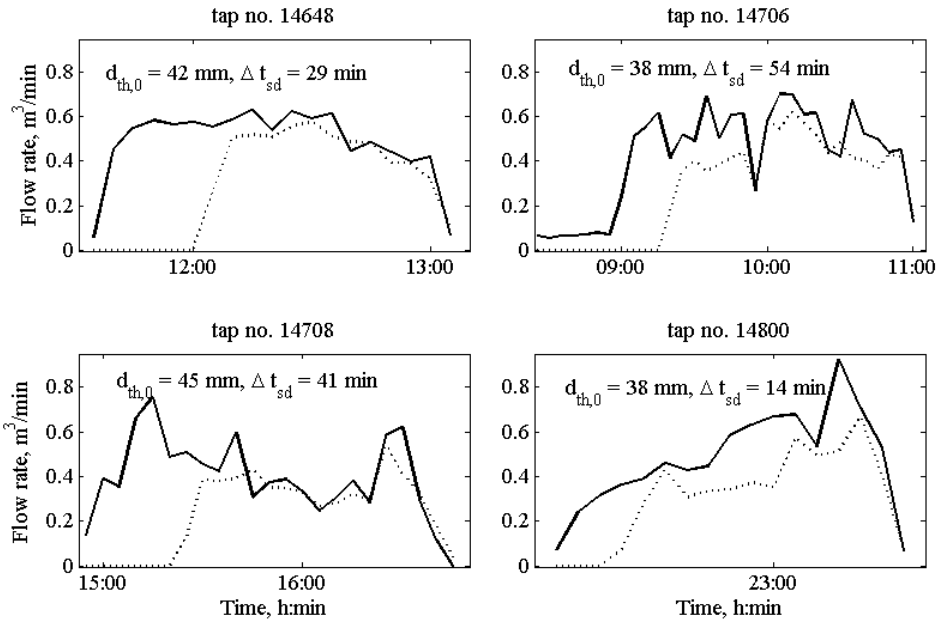

Figure 24. Outflow rates of iron (solid lines) and slag (dashed lines) for four different taps of the blast furnace studied.

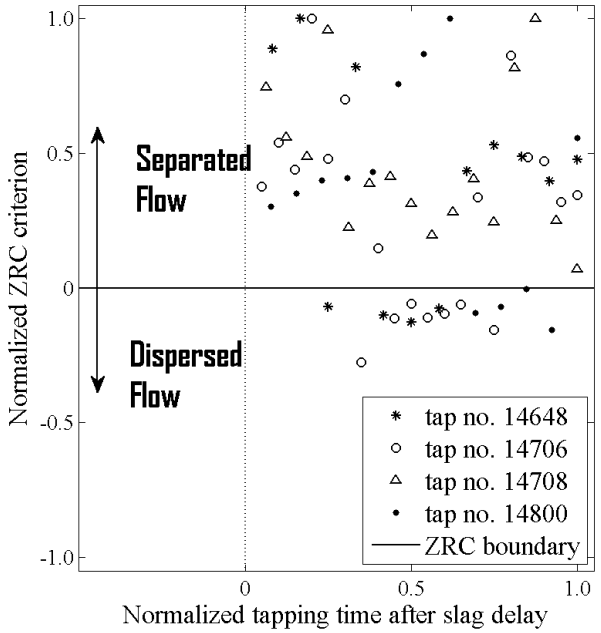

Figure 25. Calculated ZRC criteria for four different taps of the blast furnace studied. Markers correspond to liquid outflow rates which were estimated every 5 minutes during tapping.

4.5 Hearth drainage model using a two-fluid model of taphole

The overall drainage behavior of the blast furnace hearth was studied in Paper V, where a two-fluid model based on the assumption of separated flow pattern in the taphole was developed. The two-fluid model was coupled to a simple expression of pressure loss through the dead man due to fluid flow and the integrated model was demonstrated to be a useful "what-if" tool for throwing light on the evolutions of liquid outflow rates and levels in the hearth during tapping.

4.5.1 Pressure loss through dead man

In the tapping operation of the blast furnace hearth, during which the molten liquids are drained from a small taphole located at the sidewall, the driving overpressure is gradually consumed as the liquids flow towards the taphole. Shao and Saxén (2011) simulated the flow behavior of single liquid phase in an experimental hearth with a sitting dead man. The simulations showed that the streamlines converge at the taphole and almost the entire in-hearth pressure drop occurs in a quasi-hemisphere region centered at the taphole. Here, the region is assumed to be hemisphere-shaped and Kozeny-Carman equation is applied to derive the expression of pressure loss through the dead man.

The differential form of the Kozeny-Carman equation is

$$\partial p_{\mathrm{dm}} = 180 \frac{\mu}{d_{\mathrm{p}}^2} \frac{(1-\varepsilon)^2}{\varepsilon^3} U \partial r \tag{13}$$

where the subscripts "dm" stands for the dead man and r is the radial position within the hemisphere region. The liquid velocity through the surface of the hemisphere region can be expressed as

$$U = \frac{\dot{V}}{2\pi r^2} \tag{14}$$

Combing Eqs. (13) and (14) yields

$$\partial p_{\mathrm{dm}} = 180 \frac{\mu}{\pi d_{\mathrm{p}}^2} \frac{(1-\varepsilon)^2}{\varepsilon^3} \dot{V} \frac{\partial r}{2r^2} \tag{15}$$

Therefore, the overall pressure drop through the dead man can be obtained by integrating Eq. (15).

$$\Delta p_{\mathrm{dm}} = 180 \frac{\mu}{\pi d_{\mathrm{p}}^2} \frac{(1-\varepsilon)^2}{\varepsilon^3} \left(\frac{1}{2l_0} - \frac{1}{2l_1} \right) \dot{V} \tag{16}$$

In Paper V, $2l_0$ and $2l_1$ were respectively given as diameters of the taphole (R_{th}) and hearth (R_{h}) for a sitting dead man. In addition, Eq. (16) was weighed with the hydraulic diameter of each phase when considering two-phase flow through the dead man.

$$\Delta p_{\mathrm{dm,i}} = 180 \frac{\mu_{\mathrm{i}}}{\pi d_{\mathrm{p}}^2} \frac{(1-\varepsilon)^2}{\varepsilon^3} \left(\frac{1}{R_{\mathrm{th}}} - \frac{1}{R_{\mathrm{h}}} \right) \left(\frac{d_{\mathrm{i}}}{d_{\mathrm{ir}} + d_{\mathrm{sl}}} \right) \dot{V}_{\mathrm{i}}, \; i = \{\mathrm{ir}, \mathrm{sl}\} \tag{17}$$

4.5.2 Detailed analysis

The effects of coke diameter and dead-man porosity on the tap-end levels of iron and slag simulated by the model are depicted in the left panel of Fig. 26. For the slag phase, the tap-end level that reflects the residual amount of slag after the tap decreases as coke diameter and dead-man porosity rise. However, as displayed in the right panel of the figure, the end iron level becomes closer to the taphole as the two parameters increase, showing that it is impossible to reduce residual volumes of iron and slag at the same time (Nishioka et al., 2005a, b).

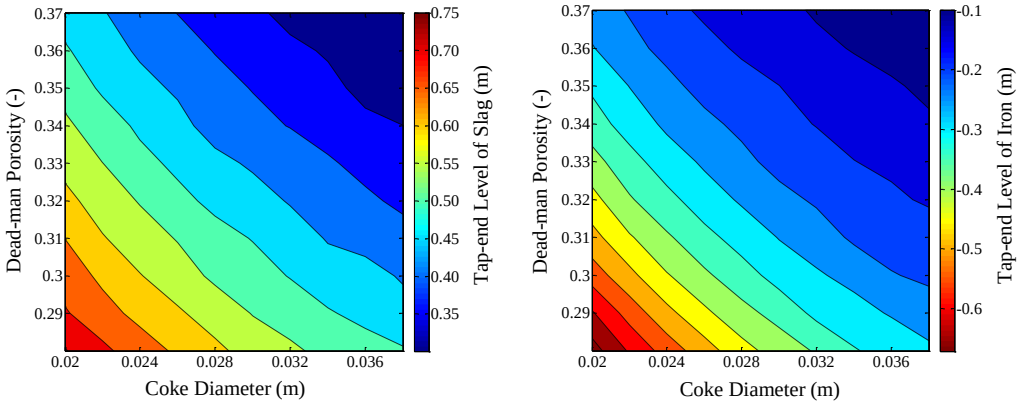

Figure 26. Effect of in-furnace conditions on the tap-end levels of slag (left) and iron (right), minus sign in the color bar means iron level below the taphole.

4.6 A promising two-fluid model for hearth flows

The two-phase flow patterns in the blast furnace hearth are also expected to be separated due to high immiscibility of iron and slag. An improved CFD model that blends the Eulerian two-fluid approach with a VOF-based interface treatment method was presented in Paper VI. The actual iron-slag system and a water-oil system, which is often used in small-scale physical models of the furnace hearth, were simulated by the two-fluid model and by the well-established VOF model. The differences between the results of the two numerical models were studied for a short-term drainage process, and the performance of the models was analyzed with respect to their predictions of the interface between the liquids and the interface angles close to the taphole.

Figure 27 plots the interface tilt angles in the two systems estimated by the (VOF and two-fluid) models and predicted with a theoretical equation presented in Paper VI. As can be seen in the left panel of Fig. 27, the taphole tilt angle estimated by the VOF model differs considerably from that given by the theoretical equation, in particular at the end of the tap. By contrast, the lower part of the left panel demonstrates that the taphole tilt angle estimated by the two-fluid model is in good agreement with that obtained by the theoretical analysis. A similar comparison of the interface angle in the water-oil system is provided in the right panel of Fig. 27. Again, the simulations by the two-fluid model

show better agreement with the theoretical predictions, even though the quality of the results of the VOF model is better than that for the iron-slag system.

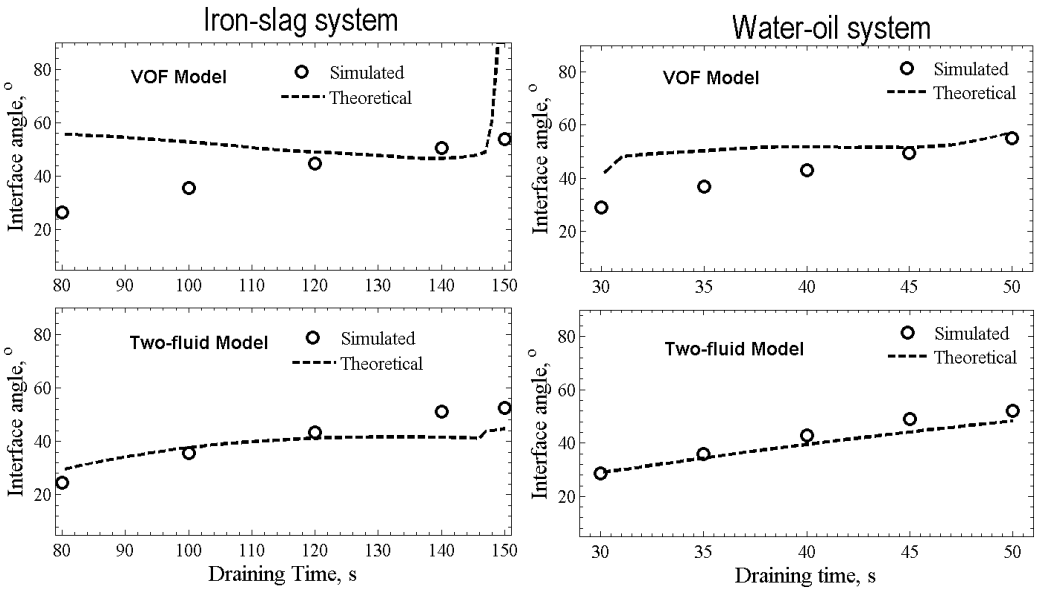

Figure 27. Tilt angles in simulations (circles, both VOF and two-fluid models) and estimated by the theoretical approximation (solid curve) for the iron-slag system (left) and water-oil system (right).

4.7 Conclusions

The main aim of this thesis was to study iron and slag flow in the blast furnace hearth and taphole. A set of models for estimating and predicting hearth drainage behavior and taphole flow patterns have been presented.

In subsections 4.1-4.2 and Paper I, a drainage model mimicking the internal conditions of a (one-taphole) blast furnace hearth was first illustrated with a couple of examples. The basis of the model was a pressure balance for the dead man. In addition, the tap-end levels of iron and slag were tuned using an asymptotic expression presented by Tanzil et al. (1984). The drainage model was later used to extract key boundary conditions including slag-iron interface and dead-man properties for a CFD model, which was performed to simulate the complicated hearth flows and to predict regions subject to

hearth erosion profile under different operating conditions. The comprehensive model also revealed a reason for the difficulties in maintaining stable state of the hearth.

In subsection 4.3 and in Paper II, an advanced drainage model for simulating hearth tap-cycle performance was described. The (initial) liquid outflow rates, which are critical inputs to the model, were computed based on the taphole diameter and length. Moreover, the tap-end levels of liquid were adjusted by using an improved relationship between the flow-out coefficient and slag residual ratio (Bean, 2008). The model was used to simulate liquid levels and dead-man state during tapping under different operating conditions. In particular, the advanced drainage model was evaluated on short-term data of the blast furnace studied, showing its ability to track the variations in slag delay and a potential way to estimate dead-man porosity at the taphole level.

In subsection 4.4 and in Papers III and IV, the simultaneous flow of iron and slag in the blast furnace taphole was investigated with different models. A VOF-based CFD model, suited for simulating the interface shape between immiscible liquids, was presented and discussed in Paper III. The calculated results showed that separated flow pattern could be dominant in the taphole when liquid outflow rates are comparable during tapping. In Paper IV, the taphole flows were further studied using a ZRC model, which is based on the stability analysis of two immiscible liquids flowing through an upwards inclined tube. The model was applied to predict the two-liquid flow pattern (i.e., separated or dispersed flow) in the taphole of the reference blast furnace. The results showed that separated flow of iron and slag more likely occurs in the furnace taphole, which is in agreement with the conclusions drawn in Paper III.

The main focus of the model presented in subsection 4.5 and in Paper V was put on building an integrated model to deepen the understanding of hearth drainage. The general idea behind the model was to calculate liquid outflow rates based on a simplified balance equation, i.e., the driving overpressure equals the flow-induced resistances through the dead man and taphole. A two-fluid model that assumes full stratification of iron and slag in the taphole (i.e., separated flow as found in the work of Paper III and Paper IV) was developed and coupled with a simple material balance of the hearth (i.e., coupling of

liquid volumes and levels as in Paper I and Paper II with sitting dead man). The model was demonstrated to be a useful tool for shedding some light on the evolutions of liquid outflow rates and levels during tapping.

In subsection 4.6 and in Paper VI, an improved CFD model, which is able to take into account interfacial forces between immiscible liquids (e.g., iron and slag), was described and evaluated. The model generally combines the Eulerian two-fluid approach with a piecewise-linear interface calculation scheme for interface tracking, which is usually applied in VOF models (as in Paper III). The interface force was demonstrated to have great impact on hearth performance in terms of liquid outflow rates and interface angle close to taphole. Thus, the improved CFD model must be considered a promising tool for estimation of hearth flows and other related processes.

Chapter 5
Future Prospects

The models presented in this thesis and the work of the papers appended have proven to be able to extract new information about iron and slag flows in the blast furnace hearth and taphole. A CFD model was presented in Paper I with the aim to deepen the understanding of iron flow and refractory erosion on the hearth bottom. An advanced drainage model was proposed in Paper II in order to consider the effects of taphole conditions on the hearth performance. The taphole flows were further studied in Papers III and IV, where different models are developed to both simulate and predict the two-liquid flow patterns in the taphole. Paper V showed an integrated tap cycle model on the basis of simple material balance in the hearth and the assumption of fully stratified flow in the taphole. Finally, an improved CFD model that is able to take into account the interfacial forces between immiscible liquids (e.g., iron and slag) was presented and evaluated in Paper VI. As the first step, the taphole flows that influence the hearth performance as a whole have been given much attention throughout this work. However, more work would be required to incorporate some or all of the models in industrial automation systems and to provide furnace operators or managers with instructive information in real-time.

Generally speaking, the models described in this thesis need to be further validated. Here, both physical experiments in laboratory and model evaluation on corresponding industrial measurements will be undertaken. The improved CFD model described in Paper VI will be utilized to conduct systematic studies of the effects of various in-furnace conditions on the drainage patterns and slag residual ratio. The model presented in Paper I can be easily extended to consider the entire process with both iron and slag phases by using the advanced model of Paper VI. Also, the UDF routine applied to reconstruct dead-man

state in the computational domain will be modified to include the transient factor, i.e., dead-man dynamics due to the accumulation and depletion of liquids during a tap cycle.

The models presented in Papers II and V can be integrated together by tuning and relaxing some parameters. The model described in Paper V can provide inputs of time-dependent outflow rates of iron and slag to the one of Paper II. At the same time, the coupling method of liquid volumes and levels proposed in Paper II can be applied to the model of Paper V to include the effect of a floating dead man. Iterative calculations will be needed in the integrating procedures. Furthermore, the pressure loss through the dead man, especially in front of the taphole, will be investigated in more detail, considering both a sitting and a floating dead man. For this purpose, some work on an integrated CFD-DEM method is already being made and the results will be reported in future. Another interesting use of the integrated model is to estimate dead-man porosity at the taphole level on the basis of measured slag delay and taphole conditions.

The models presented in Paper III will be updated to reflect the “real” geometry of a taphole. For instance, the taphole entrance shape and gradual expansion in size caused by erosion will be considered. The ZRC model described in Paper IV will be further evaluated on a set of filtered process data.

Finally, it should be noted that some of the models were established with a typical tap cycle of the reference one-taphole blast furnace in mind, where there is a well-defined inter-tap period. However, the models could be implemented at any blast furnace with some minor adjustments, but the concept of using the slag delay as a signal for model verification should then be revised.

Nomenclature

Roman Letters

a	Parameter of Eq. (1) (kPa)
A	Area (m^2)
C	Criterion (-)
d	Effective coke/ diameter (m/mm)
D	Hearth diameter (m)
F_L / F_L^*	Flow-out coefficient (-)
g	Gravitational acceleration (m/s^2)
i	Iron or slag
j	Iron or slag
k	Tap number (-)
l	Distance/Length (m)
$\dot{m}$	Production rate (t/d)
n	Parameter of Eq. (1) (-)
p	Pressure (kPa)
$\bar{p}_d$	Parameter of Eq. (1) (kPa)
r	Radial position (m)
R	Parameter of Eq. (1)/Radius (m)
Re	Reynolds number (-)
t	Time (min)
U	Superficial/Mean velocity (m/s)
V	Volume (m^3)
$\dot{V}$	Volumetric flow rate (m^3/min)
z	Vertical level/height (m)

Greek Letters

α	Slag residual ratio (-)
ε	Dead-man porosity (-)
μ	Viscosity (Pa·s)
ρ	Density (kg/m^3)
σ	Parameter of Eq. (12) (-)

Subscripts

0	Initial value/Start of iron flow
b	Buoyancy
cf	Coke-free zone
d	Downward-acting
e	Tapping end

dm	Dead-man
fl	Flow
ft	Far-taphole
h	Hearth
hb	Hearth bottom
i	Iron or slag
in	Inflow
ir	Iron
j	Iron or slag
out	Outflow
p	Particle
pl	Plugging
prod	Production
sd	Slag delay
sl	Slag
ss	Slag-start
th	Taphole
zrc	Zero real characteristic

Superscript

max	Maximum

Operators

d	Differential
∂	Partial differential
Δ	Difference

References

Bean, I. (2008). *Blast Furnace Hearth Drainage Improvement of the Residual-Flowout Correction*. Master Thesis, University of New South Wales, Sydney, Australia.

Brauner, N and Maron, D. M. (1992a). Stability Analysis of Stratified Liquid-Liquid Flow. *Int. J. Multiphase Flow*, Vol. 18, pp. 103-121.

Brauner, N and Maron, D. M. (1992b). Flow Pattern Transitions in Two-Phase Liquid-Liquid Flow in Horizontal Tubes. *Int. J. Multiphase Flow*, Vol. 18, pp. 123-140.

Brännbacka, J. and Saxén, H. (2001). Modeling the Liquid Levels in the Blast Furnace Hearth. *ISIJ Int*., Vol. 41, pp. 1131-1138.

Brännbacka, J. and Saxén, H. (2003). Model Analysis of the Operation of the Blast Furnace Hearth with a Sitting and Floating Dead Man. *ISIJ Int*., Vol. 43, pp. 1519-1527.

Brännbacka, J. (2004). *Model Analysis of Dead-man Floating State and Liquid Levels in the Blast Furnace Hearth*. Doctoral Thesis, Åbo Akademi University, Turku, Finland.

Brännbacka, J., Torrkulla, J. and Saxén, H. (2005). Simple Simulation model of Blast Furnace Hearth. *Ironmaking and Steelmaking*, Vol. 32, pp. 479-486.

Brännbacka, J. and Saxén, H. (2008). Model for Fast Computation of Blast Furnace Hearth Erosion and Buildup Profiles. *Ind. Eng. Chem. Res.*, Vol. 47, pp. 7793-7801.

Dash, S. K., Ajmani, S. K., Kumar, A. and Sandhu, H. S. (2001). Optimum Taphole Length and Flow Induced Stresses. *Ironmaking and Steelmaking*, Vol. 28, pp. 110-116.

Dash, S. K., Jha, D. N., Ajmani, S. K. and Upadhyaya, A. (2004). Optimisation of Taphole Angle to Minimise Flow Induced Wall Shear Stress on the Hearth. *Ironmaking and Steelmaking*, Vol. 31, pp. 207-215.

Desai, D. (1993). Analysis of Blast Furnace Hearth Drainage Based on the Measurement of Liquid Pressure inside of the Hearth. *Transaction of the Iron & Steel Society of AIME*, Vol. 14, pp. 45-50.

Fukutake, T. and Okabe, K. (1974). Investigation of Slag Flow in the Blast Furnace Hearth Based on the Fluid Dynamics and of Relation between Residual Slag Amount and Tapping Out Conditions. *Trans. ISIJ*, Vol. 60, pp. 607-621.

Fukutake, T. and Okabe, K. (1976a). Experimental studies of Slag Flow in the Blast Furnace Hearth during Tapping Operation. *Trans. ISIJ*, Vol. 16, pp. 309-316.

Fukutake, T. and Okabe, K. (1976b). Influences of Slag Tapping Conditions on the Amount of Residual Slag in Blast Furnace Hearth. *Trans. ISIJ*, Vol. 16, pp. 317-323.

Guo, B. Y., Yu, A. B., Wright, B. and Zulli, P. (2006). Simulation of Turbulent Flow in a Packed Bed. *Chem. Eng. Technol.*, Vol. 29, pp. 596-603.

Guo, B. Y., Maldonado, D., Zulli, P. and Yu, A. B. (2008). CFD Modelling of Liquid Metal Flow and Heat Transfer in Blast Furnace Hearth. *ISIJ Int.*, Vol. 48, pp. 1676-1685.

He, Q., Zulli, P., Tanzil, F., Lee, B., Dunning, J. and Evans, G. (2002). Flow Characteristic of a Blast Furnace Taphole Stream and its Effects on Trough Refractory Wear. *ISIJ Int.*, Vol. 42, pp. 235-242.

He, Q., Zulli, P., Evans, G. M. and Tanzil, F. (2006). Free Surface Instability and Gas Entrainment during Blast Furnace Drainage. *Dev. Chem. Eng. Mineral Process*, Vol. 14, pp. 249-258.

Iida, M., Ogura, K. and Hakone, T. (2008). Analysis of Drainage Rate Variation of Molten Iron and Slag from Blast Furnace during Tapping. *ISIJ Int.*, Vol. 48, pp. 412-419.

Iida, M., Ogura, K. and Hakone, T. (2009). Analysis of Numerical Study on Metal/Slag Drainage Rate Deviation during Blast Furnace Tapping. *ISIJ Int.*, Vol. 49, pp. 1123-1132.

Inada, T., Takatani, K., Miyahara, M., Wakabayasi, S., Yamamoto, T., Kasai, A. and Takata, K. (1999). Development and Application of an Advanced Numerical Analysis Technology for Blast Furnace Hearth. *Proc. ISS Ironmaking Conf.*, pp. 633-639.

Inada, T., Kasai, A., Nakano, K., Komatsu, S. and Ogawa, A. (2009). Dissection Investigation of Blast Furnace Hearth – 2nd Campaign. *ISIJ Int.*, Vol. 49, pp. 470-478.

Jameson, D. and Eden, M. G. (1999). The Taphole Zone – the Critical Factor in Long Campaign Life. *Ironmaking Conf. Proc.*, pp. 625-631.

Kanbara, K., Hagiwara, T., Shigemi, A., Kondo, S., Kanayama, Y., Wakabayashi, K. and Hiramoto, N. (1977). Dissection of Blast Furnaces and Their Internal State. *Trans. ISIJ*, Vol. 17, pp. 371-380.

Kasai, A., Kiguchi, J., Kamijo, T. and Shimizu, M. (1998). Degradation of Coke by Molten Iron Oxide in the Cohesive Zone and Dripping Zone of a Blast Furnace. *Tetsu-to-Hagané*, Vol. 84, pp. 9-13.

Kawai, H. and Takahashi, H. (2004). Solid Behavior in Shaft and Deadman in a Cold Model of Blast Furnace with Floating-Sinking Motion of Hearth Packed Bed Studied by Experimental and Numerical DEM Analyses. *ISIJ Int*., Vol. 44, pp. 1140-1149.

Kowalski, W., Bachofen, H. J., Rüther, H. P., Rödl, S. and Marx, K. (1998). Investigation on Tapping Strategies at the Blast Furnace with Special Regard to the State of the Hearth. *Proc. ISS Ironmaking Conf*., pp. 595-606.

Kumar, S. (2005). Heat Transfer Analysis and Estimation of Refractory Wear in an Iron Blast Furnace Hearth using Finite Element Method. *ISIJ, Int.*, Vol. 45, pp. 1122-1128.

Liu, Z. J., Zhang, J. L., Zuo, H. B. and Yang, T. J. (2012). Recent Progress on Long Service Life Design of Chinese Blast Furnace Hearth. *ISIJ, Int.*, Vol. 52, pp. 1713-1723.

Nightingale, R. J. and Tanzil, F. W. B. U. (1997). A Novel Approach in the Estimation of Blast Furnace Hearth Voidage. *Iron & Steelmaker*, February, pp. 35-37.

Nightingale, R. J., Tanzil, F. W. B. U., Beck, A. J. G. and Price, K. (2001). Blast Furnace Hearth Condition Monitoring and Taphole Management Techniques. *La Revue de Métallurgie-CIT*, Vol. 98, pp. 533-540.

Nishio, H., Wenzel, W. and Gudenau, H. W. (1977). The Significance of the Dead Zone in the Blast Furnace. *Stahl und Eisen*, Vol. 97, pp. 867-875.

Nishioka, K., Maeda, T. and Shimizu, M. (2005a). A Three-dimensional Mathematical Modelling of Drainage Behavior in Blast Furnace Hearth. *ISIJ Int*., Vol. 45, pp. 669-676.

Nishioka, K., Maeda, T. and Shimizu, M. (2005b). Effect of Various In-furnace Conditions on Blast Furnace Hearth Drainage. *ISIJ Int*., Vol. 45, pp. 1496-1505.

Nouchi, T., Yasui, M. and Takeda, K. (2003). Effects of Particle Free Space on Hearth Drainage Efficiency. *ISIJ Int.*, Vol. 43, pp. 175-180.

Nouchi, T., Sato, M., Takeda, K. and Ariyama, T. (2005). Effects of Operation Condition and Casting Strategy on Drainage Efficiency of the Blast Furnace Hearth. *ISIJ Int.*, Vol. 45, pp. 1515-1520.

Nouchi, T., Sato, M. and Takeda, K. (2009). Process Analysis for Blast Furnaces by the Discrete Element Method. *JFE Technical Report*, No. 13, pp. 28-33.

Ohno, J., Tachimori, M., Nakamura, M. and Hara, Y. (1985). Influence of Hot Metal Flow on the Heat Transfer in a Blast Furnace Hearth. *Tetsu-to-Hagané*, Vol. 71, pp. 34-40.

Omori, Y. (ed.) (1987). *Blast Furnace Phenomena and Modelling*. ISIJ, Elsevier, London.

Panjkovic, V., Truelove, J. S. and Zulli, P. (2002). Numerical Modelling of Iron Flow and Heat Transfer in Blast Furnace Hearth. *Ironmaking and Steelmaking*, Vol. 29, pp. 390-400.

Preuer, A. and Winter, J. (1993). Numerical Simulation of Refractory Erosion Caused by Carbon Dissolution in Blast Furnace. *La Revue de Métallurgie - CIT*, Vol. 90, pp. 955-963.

Raipala, K. (2003). *On Hearth Phenomena and Hot Metal Carbon Content in Blast Furnace*. Doctoral Thesis, Helsinki University of Technology, Helsinki, Finland.

Shao, L. and Saxén, H. (2011). Pressure Drop in the Blast Furnace Hearth with a Sitting Deadman. *ISIJ Int*., Vol. 51, pp. 1014-1016.

Shibata, K., Kimura, Y., Shimizu, M. and Inaba, S. (1990). Dynamics of Dead-Man Coke and Hot Metal Flow in a Blast Furnace Hearth. *ISIJ Int.*, Vol. 30, pp. 208-215.

Shibata, K., Kimura, Y., Shimizu, M. and Inaba, S. (1991). Control of Hot Metal Flow in Blast Furnace Hearth by Blasting and Drainage. *Proc. McMaster Symp. Iron and Steelmaking*, pp. 118-140.

Shinotake, A., Ichida, M., Ootsuka, H. and Kurita, Y. (2003). Bottom Shape of Blast Furnace Deadman and its Floating/Sinking Behavior by 3-dimensional Model Experiment. *Tetsu-to-Hagané*, Vol. 89, pp. 77-84.

Sun, H. (2005). Analysis of Reaction Rate between Solid Carbon and Molten Iron by Mathematical Models. *ISIJ Int*., Vol. 45, pp. 1482-1488.

Sunahara, K., Inada, T. and Iwanaga, Y. (1993). Size Degradation of Deadman Coke by Reaction with Molten FeO in Blast Furnace. *ISIJ Int*., Vol. 33, pp. 275-283.

Stevenson, P. and He, Q. (2005). Slug Flow in a Blast Furnace Taphole. *Chemical Engineering and Processing*, Vol. 44, pp. 1094-1097.

Swartling, M., Sundelin, B., Tilliander, A. and Jönsson, P. (2010). Short-term Lining Temperature Changes during Tapping in a Blast Furnace. *Steel Research Int*., Vol. 81, pp. 724-734.

Swartling, M., Tilliander, A., Saxén, H. and Jönsson, P. (2012). Interpretation of Tap Induced Cyclic Temperatures in the Blast Furnace Lining. *Steel Research Int*., Vol. 83, pp. 695-704.

Takahashi, H. and Komatsu, N. (1993). Cold Model Study on Burden Behaviour in the Lower Part of Blast Furnace. *ISIJ Int.*, Vol. 33, pp. 655-663.

Takahashi, H., Tanno, M. and Katayama, J. (1996). Burden Descending Behavior with Renewal of Deadman in a Two Dimensional Cold Model of Blast Furnace. *ISIJ Int.*, Vol. 36, pp. 1354-1359.

Takahashi, H., Kawai, H. and Suzuki, Y. (2002). Analysis of Stress and Buoyancy for Solids Flow in the Lower Part of a Blast Furnace. *Chemical Engineering Science*, Vol. 57, pp. 215-226.

Takeda, K., Watakabe, S., Sawa, Y., Itaya, H., Kawai, T. and Matsumoto, T. (1999). Prevention of Hearth Brick Wear by Forming a Stable Solidified Layer. *Proc. ISS Ironmaking Conf.*, pp. 657-665.

Tanzil, W. B. U., Zulli, P., Burgess, J. M. and Pinczewski, W. V. (1984). Experimental Model Study of the Physical Mechanisms Governing Blast Furnace Hearth Drainage. *Trans. ISIJ*, Vol. 24, pp. 197-205.

Tanzil, W. B. U. (1985). *Blast Furnace Hearth Drainage*. Doctoral Thesis, University of New South Wales, Sydney, Australia.

Tanzil, W. B. U. and Pinczewski, W. V. (1987). Blast Furnace Hearth Drainage: Physical Mechanisms. *Chemical Engineering Science*, Vol. 42, pp. 2557-2568.

Tanzil, W. B. U. F., Nightingale, S. A. and Nightingale, R. J. (2001). Predicting the Effect of Taphole Clay Degradation on Liquid Flow from a Blast Furnace. *Proc. ISS Ironmaking Conf.*, pp. 893-901.

Tanzil, W. B. U., Nightingale, R. J., Zulli, P., Wright, B. D. and Bean, I. (2004). Improved Blast Furnace Casting Performance through Implementation of Hearth Drainage Mathematical and Physical Models. *SCANMET II – 2nd International Conference on Process Development in Iron and Steelmaking*, Luleå, Sweden, pp. 321-332.

Torrkulla, J. and Saxén, H. (2000). Model of the State of the Blast Furnace Hearth. *ISIJ Int.*, Vol. 40, pp. 438-447.

Tsuchiya, N., Fukutake, T., Yamauchi, Y. and Matsumoto, T. (1998). In-furnace Conditions as Prerequisites for Proper Use and Design of Mud to Control Blast Furnace Taphole Length. *ISIJ Int*., Vol. 38, pp. 116-125.

Vats, A. K. and Dash, S. K. (2000). Flow Induced Stress Distribution on Wall of Blast Furnace Hearth. *Ironmaking and Steelmaking*, Vol. 27, pp. 123-128.

Vogelpoth, H. B., Still, G. and Peters, M. (1985). Estimations Concerning the Flow Behavior of Hot Metal in Blast Furnace. *Stahl und Eisen*, Vol. 105, pp. 451-457.

Zhang, S. J., Yu, A. B., Zulli, P., Wright, B. and Austin, P. (2002). Numerical Simulation of Solids Flow in a Blast Furnace. *Applied Mathematical Modelling*, Vol. 26, pp. 141-154.

Zulli, P. (1991). *Blast Furnace Hearth Drainage With and Without Coke-Free Layer*. Doctoral Thesis, University of New South Wales, Sydney, Australia.

Zulli, P., Tanzil, F. W. B. U, He, Q., Wright, B. D., Bean, I. and Nightingale, R. J. (2003). Blast Furnace Hearth Drainage – Implementing Fundamental Knowledge. *Proc. 3rd International Conference on Science and Technology of Ironmaking (ICSTI)*, Dusseldorf, Germany, pp. 482-490.

ISBN 978-952-12-2941-1
Painosalama Oy – Turku, Finland 2013